ELSEVIER

Coordination Chemistry Reviews
178–180 (1998) 1433–1484

COORDINATION CHEMISTRY REVIEWS

Metallophthalocyanines
Gas sensors, resistors and field effect transistors[1]

G. Guillaud [a], J. Simon [b,*], J.P. Germain [c]

[a] *Université C. Bernard, 43 boulevard du 11 novembre 1918, F-69622 Villeurbanne, France*
[b] *ESPCI-CNRS, 10 rue Vauquelin, F-75231 Paris, Cedex 05, France*
[c] *Université B. Pascal, 24 Avenue des Landais, F-63177 Aubière, Cedex, France*

Received 17 March 1998; accepted 1 July 1998

Contents

Abstract

The conventional metallophthalocyanines (PcM, M=Cu, Zn, Ni …) are insulators when undoped. However, they possess accessible π and π* orbitals which make at least partial oxidization or reduction of the macrocycle possible with gases such as NO_2 or O_3. This yields more or less conductive molecular materials. Their resistance is, therefore, a measurement of the concentration of the oxidizing or reducing species present in the surrounding atmosphere (resistors). In the case of rare earth bisphthalocyanines (in particular the lutetium derivative), the intrinsic density of charge carriers is no longer negligible and the corresponding thin films

* Corresponding author. Fax: +33 01 40794425; e-mail: jacques.simon@espci.fr
[1] In memory of Christine Maleysson.

PII S0010-8545(98)00177-5

or crystals are semiconductors. Gases such as NO_2, at moderate concentrations and temperatures, can afford completely oxidized materials: the doping process which increases the conductivity is therefore followed by an increase in the resistance.

The same type of studies have been carried out using metallophthalocyanine as the electroactive (semiconductive) part of a field effect transistor (FET). After a schematic description of the chemical phenomena arising in molecular FET, a detailed chronology of their discovery is given. The influence of gases on FET characteristics is then reported.

Keywords: Field effect transistor; Gas sensors; Phthalocyanines; Resistors

1. Introduction

Phthalocyanines (from the Greek naphtha and cyanide, rockoil and dark blue) are colorants which have been known for many years. The first phthalocyanine was produced accidentally in 1907 during a study of the properties of 1,2-cyanobenzamide. On heating an alcoholic solution of the benzamide, a highly insoluble blue product precipitated [1]. Twenty years later, a copper phthalocyanine was obtained during an attempted preparation of 1,2-dicyanobenzene from dibromobenzene and CuCN [2]. However, it was Linstead and coworkers in the 1930s who fitted these earlier observations into a systematic scheme showing that a vast range of phthalocyanines were all based on the structure shown in Fig. 1 [3]. A huge number of different metallophthalocyanines (abbreviated as PcM) have been produced and studied, with a concomitant large literature of tens of thousands of publications. Apart from their uses as dyes or pigments, PcMs show a number of special properties which account for the great interest they have always aroused.

– They are easily crystallized and sublimed, resulting in materials of a purity (10^{14}–10^{16} traps cm^{-3}) which is rare in molecular chemistry.

– They show an exceptional thermal and chemical stability. In air PcMs undergo no noticeable degradation up to several hundred degrees centigrade and in vacuum most complexes do not decompose below 900 °C [4]. Strong acids (conc. H_2SO_4) or strong bases do not affect conventional PcMs. Only very strong oxidizing agents (dichromate or ceric salts) can break the molecules down to phthalimide or phthalic acid [3,5].

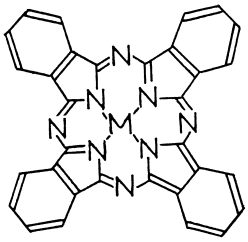

Fig. 1. Molecular structure of metallophthalocyanines. Abbreviation used: PcM.

– They show remarkable optical properties. The conjugated π system, containing 18 electrons, leads to very intense absorption bands in the visible at 400 nm and 700 nm with extinction coefficients of the order of 2×10^5 l mol^{-1} cm^{-1} in solution.
– They provide a versatile chemical system. Elements from groups I_A to V_B can all combine with the phthalocyanine ring and more than 70 different PcMs are known.

The nature of the sequestered metal ions has an influence on the physicochemical properties of the PcM. For example, the oxido–reduction behavior of the molecular unit or the nature of the photochemical excited state may be altered by changing the metal ion in the complex. By varying substituents on the ring, the range of properties of the PcMs may be expanded even further.

Monographs on the general properties of metallophthalocyanine are available in the literature [6–10].

Metallophthalocyanines — mostly PcCu — are produced in industry on a very large scale: around 50 000 tons per year. The commercial price of PcCu (crude grade) is approximately 30 FF per kg. PcMs are used as pigments and dyes when properly substituted. However, PcMs are also utilized in photocopying machines as photoconductors: not only their tinctorial strength is employed in industry.

In the following, only the electrical properties of thin films of metallophthalocyanines will be studied. It will be seen that the structure and the morphology of the

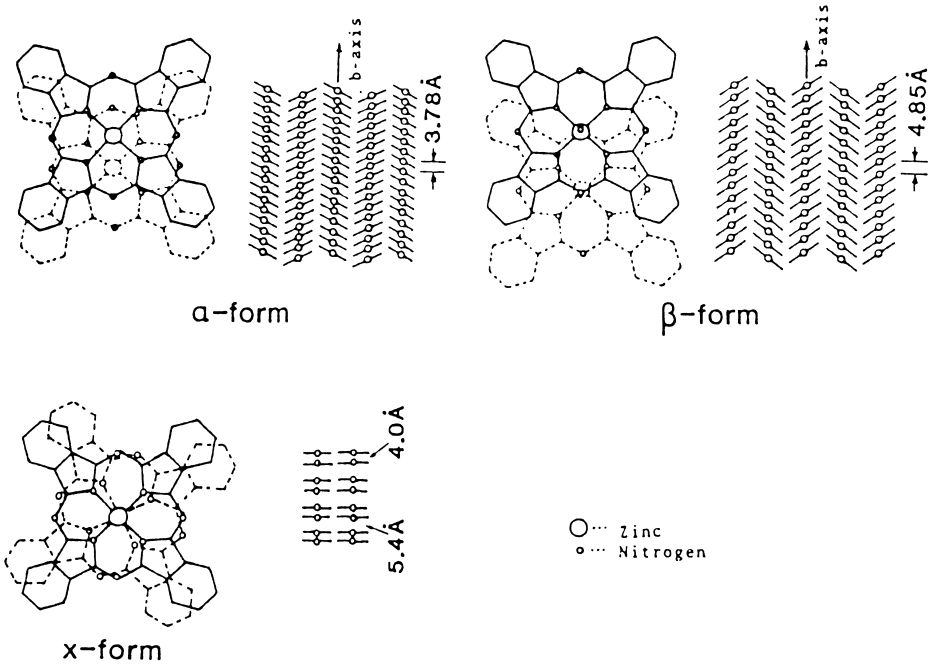

Fig. 2. Schematic representation of the three main molecular stackings found for PcZn, which is representative of metallophthalocyanines (after Refs. [15–17]).

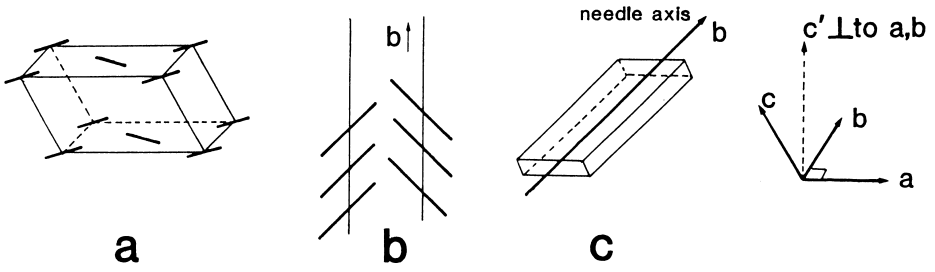

Fig. 3. Basic parameters of the lattice of β-PcH_2: (a) unit cell; (b) stacking in the *ab* plane; (c) needle axis.

molecular material have a drastic influence on the physicochemical properties of the films.

2. Metallophthalocyanines: thin film morphology

Since 1935, the structures of most of the PcMs have been determined from X-ray diffraction measurements [11–14]. At least three polymorphic forms are known, being designated by the letters α, β and x (Fig. 2).

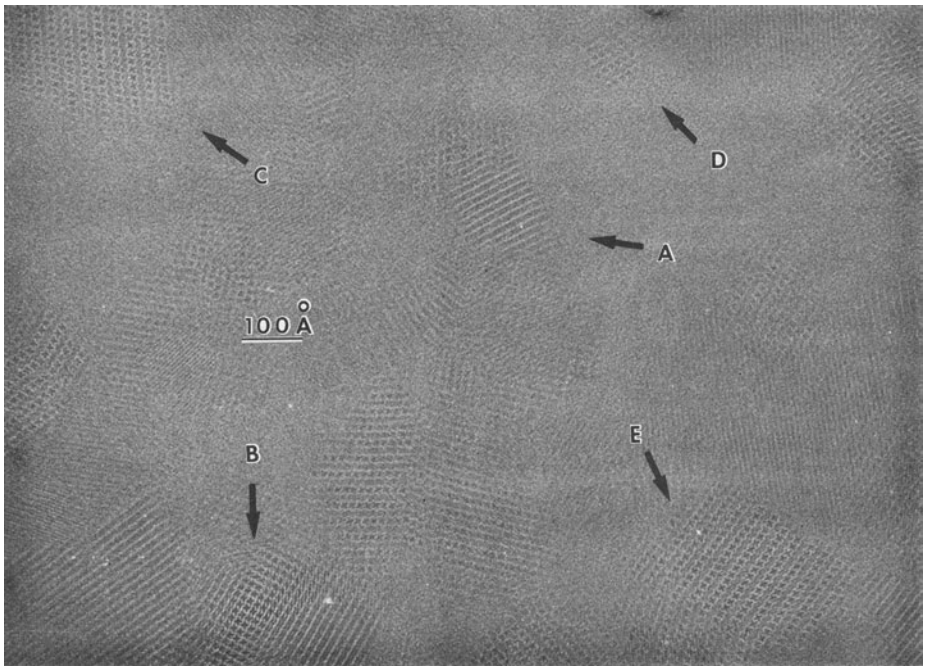

Fig. 4. Electron micrograph of a PcZn thin film (see text for the conditions). (After Ref. [23] with the permission of the International Union of Crystallography.)

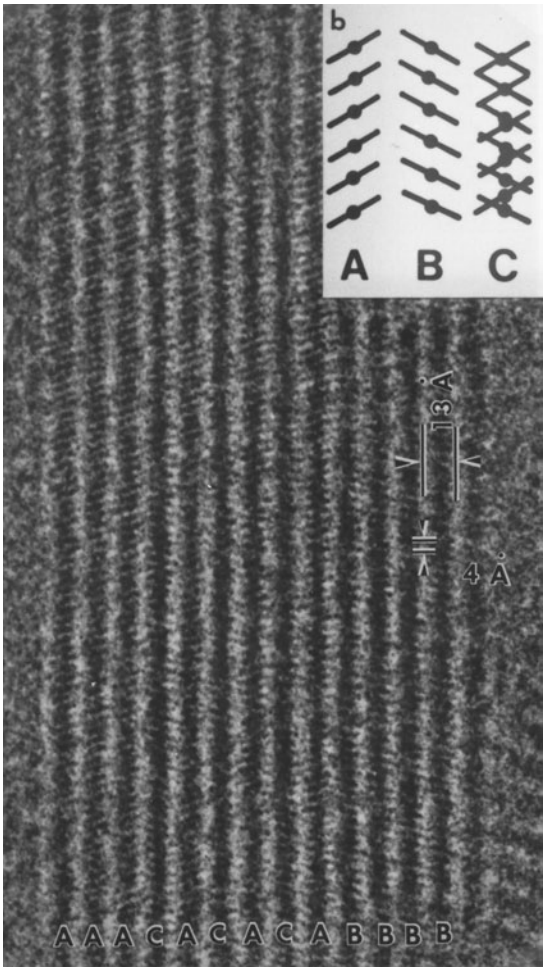

Fig. 5. High resolution image showing stacking along the *b*-axis (after Ref. [23]).

Large-size single crystals are, in most cases, of the β type. They are generally grown by sublimation under a stream of nitrogen (7 Torr) at a temperature in the range 400–500 °C. The crystals are needle-shaped, typically 1 cm long, 0.1 cm wide and 0.01 cm thick. PcMs crystallize in a base-centered monoclinic lattice. The large-area surfaces are (001) faces, and the needle direction is the *b*-axis (Fig. 3).

PcMs form polycrystalline films of the α type [18–22] when evaporated under vacuum (10^{-5}–10^{-6} Torr) onto a substrate maintained at room temperature. More detailed studies have been carried out in the case of vacuum-deposited films of PcZn [23]. The rate of deposition was 0.5 Å s^{-1} onto a carbon substrate maintained at room temperature, and the film thickness was around 50 Å. The corresponding pressure was 5×10^{-7} Torr. High-resolution electron micrographs of PcZn films show that the film is composed of crystallites whose sizes do not exceed 300 Å

(Fig. 4). Several forms differing by the relative orientation of the macrocycles between adjacent columns may be distinguished. It can be seen that the stacking sequence is not uniform: the major part can be represented as AAA and some as ABA or ACA (Fig. 5).

At least three different polymorphs can be observed on the electron micrographs [23]:

		a (Å)	*c* (Å)
α-I	PcZn	26.0	24.0
α-II	PcZn	26.0	26.0
α-III	PcZn	13.0	26.0

It is also possible to obtain amorphous (or quasi-amorphous) thin films of PcM by sublimation on a substrate maintained at low temperatures (liquid nitrogen) [24]. Crystallization to the α-phase occurs between 50 and 140 °C. Further heating at 200 °C irreversibly transforms the material into the β form. The pressure within the vacuum chamber and the deposition rate influence to a large extent the properties of the metallophthalocyanine thin films [25]. In particular, the density of the thin films is dependent on the pressure used for deposition [26] (Table 1).

Experiments on PcH_2 have shown that the substrate temperature greatly influences the molecular arrangement relative to the substrate [27].

Very detailed studies on the crystal defects which can occur in phthalocyanine thin films have been carried out [28]. Planar defects have been observed as stacking faults or grain boundaries (Fig. 6). An example of planar defect associated with a grain boundary can be seen in Fig. 7. The molecular orientation in the upper side of the boundary is different relative to the lower part. The molecules on the line XX′ have a different orientation from the molecules belonging to both the lower and upper parts [28].

Twin formation may also occur where the crystal is composed of two kinds of molecular layer which have different molecular orientations. It can be seen in Fig. 8(A) that in the left and right parts of the crystal, the direction of the *a*-axis is reversed with the *c*-axis remaining the same. The growth of the twin structure can be understood by considering that the addition of an extra molecular unit can occur in two ways, as shown in Fig. 8(B).

It will be seen in further sections that the nature and quantity of defects highly influence the gas sensor properties of the metallophthalocyanine thin films.

The rate of transformation of the α-form to the β-form is influenced by the presence of an alcohol atmosphere [15]. At the same time, the size of the crystallite

Table 1
Density of PcCu thin films as a function of the pressure within the vacuum chamber during deposition [26]

Pressure (Torr)	Density ($g\,cm^{-3}$)
10^{0}–10^{1}	1.615
10^{-1}–10^{-2}	1.637
10^{-3}–10^{-6}	1.641

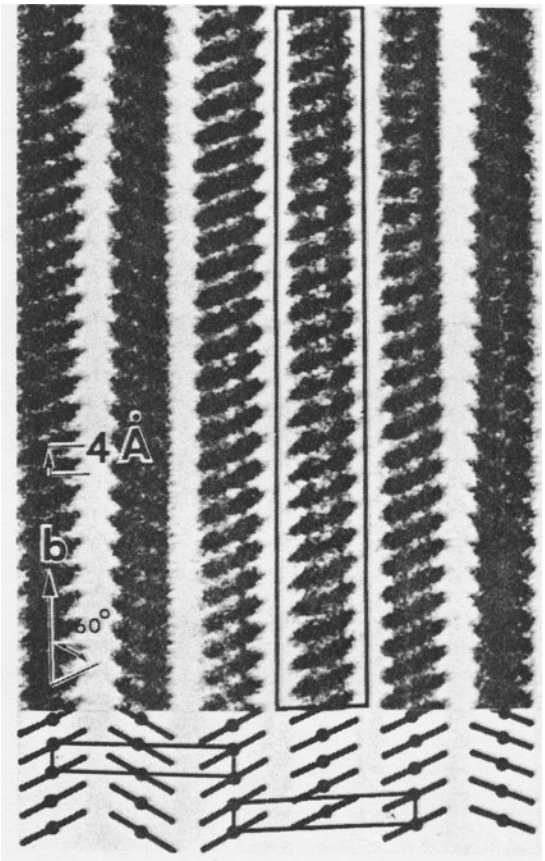

Fig. 6. Stacking fault: projection of the image of a PcZn thin film. The column enclosed is misoriented and shifted by a half period along the *b*-axis (after Ref. [28]).

drastically changes from 100–200 Å in the α-phase to 10 000–20 000 Å in the β-phase. In this last case, long needles can be formed [29,30].

The x-modification is obtained from the α-form by neat-milling [17].

The previous results have been obtained with metal-free or small divalent ion complexes of phthalocyanine. In these cases the macrocyclic ring is planar to within 0.3 Å and the symmetry of the molecular unit is D_{4h} (or D_{2h} for PcH_2). The metal–nitrogen bond is, in most cases, between 1.8 and 2.0 Å long.

Most of the divalent transition metals have ionic radii of the order of 0.7–0.8 Å and can form in-plane complexes. Out-of-plane metal complexes may be formed when the size of the metallic ion exceeds the size of the macrocyclic cavity available. Pb^{2+}, which has an ionic radius of 1.20 Å, forms out-of-plane complexes with the phthalocyanine ligand [31,32].

Two crystalline forms of PcPb are known (Fig. 9). In the monoclinic form, PcPb molecules are packed in columns, the Pb atoms forming a one-dimensional chain. In the triclinic form, two independent molecular columns exist in the crystal.

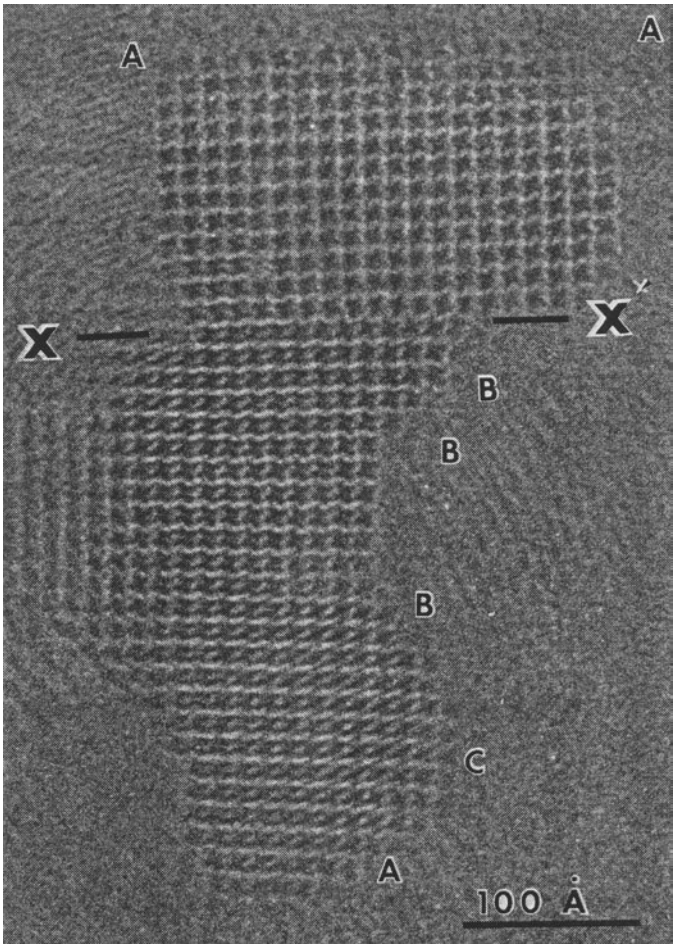

Fig. 7. Grain boundary occuring along the line XX′ [28].

The Pb–N distance is different in the two crystalline forms, 2.36 Å for the triclinic and 2.21 Å for the monoclinic form. Another monoclinic modification has been described [33,34].

Six-coordinate tetragonal and five-coordinate square pyramidal complexes are possible by axial ligation of various molecules (Fig. 10) [35].

Five- or six-coordinate species very probably intervene in the gas sensor properties of the devices.

3. Gas sensors based on conductivity measurements (resistors)

The term ‘‘chemiresistor’’ was proposed in 1960 to designate a device in which a resistance varies by exposure to a chemical substance [46].

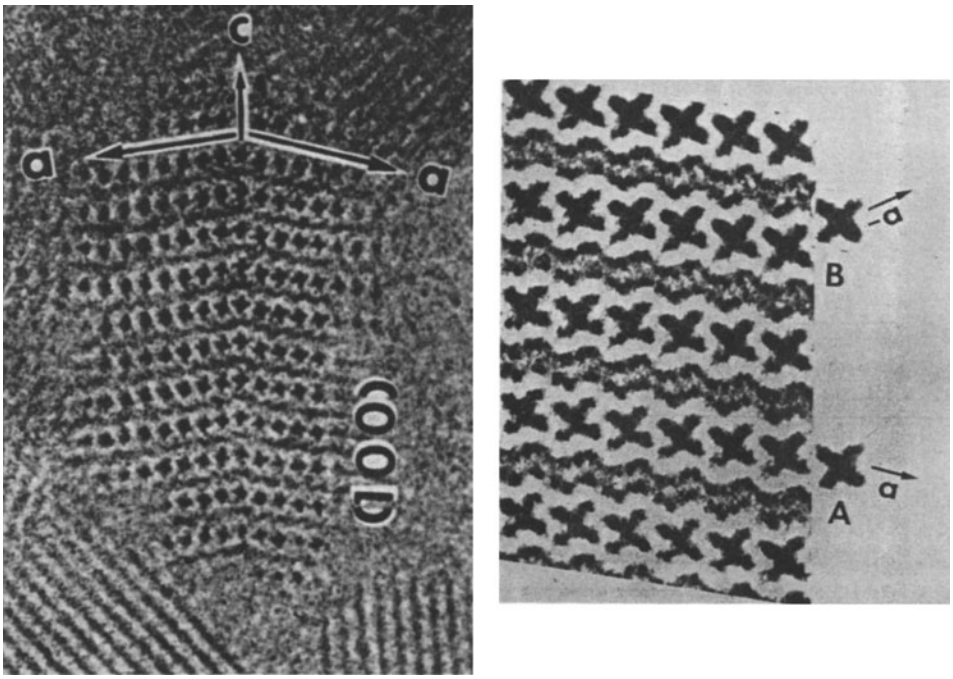

Fig. 8. (A) Twin structure (the *c*-axis is conserved but the orientation of the *a*-axis is different). (B) Twin formation: an extra PcM molecule can add in the A or B position. In the last case twin formation occurs (after Ref. [28]).

3.1. Generalities

Even a very simple and incomplete description of the interaction between gases and molecular materials requires us to take into account many elementary physico-chemical processes (Fig. 11).

The very first step of the detection of a gas is the adsorption of the molecule on the surface of the material. In many cases, the surface is already covered by another type of molecule, less firmly bound — usually dioxygen — and this latter must be removed to allow the adsorption of a new molecule. The basis of such a process was given by Langmuir in 1916 [36].

If there are n molecules per unit volume, in a given time t, only those situated at a distance $l \leq v_x t$ of a surface can reach the surface. If the corresponding surface area is A, the total number of collisions is:

$$v_x t A n \quad (\text{or } v_x A n \text{ per second})$$

where v_x is the velocity along the x vector. The pressure is equivalent to a force per surface unit which is in turn related to a momentum mv_x per unit time. The pressure is therefore given by the product: momentum times number of collisions per surface unit:

$$F = (2mv_x)(nv_x A) \tag{1}$$

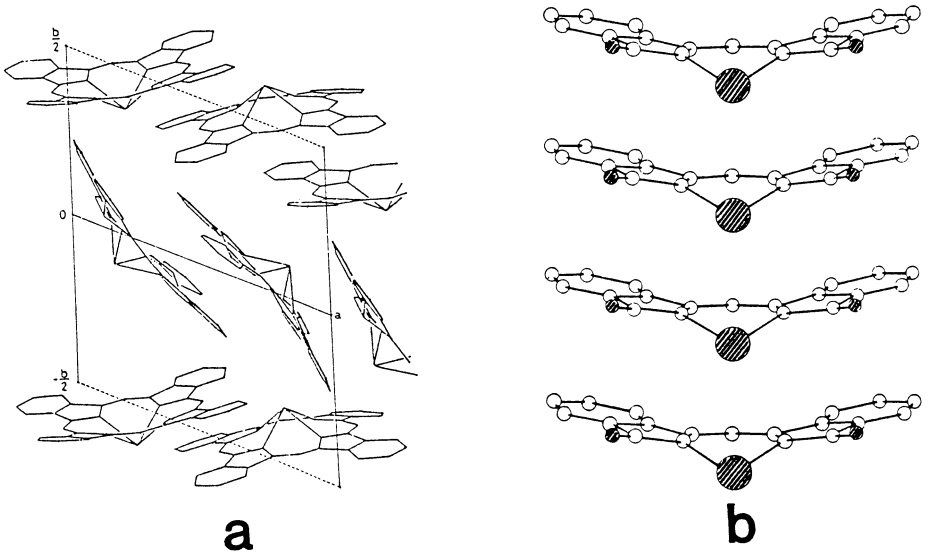

Fig. 9. Crystal structures of the triclinic and monoclinic forms of PcPb (modified from Refs. [31,32]): (a) triclinic form, projection onto the (001) plane; (b) monoclinic form.

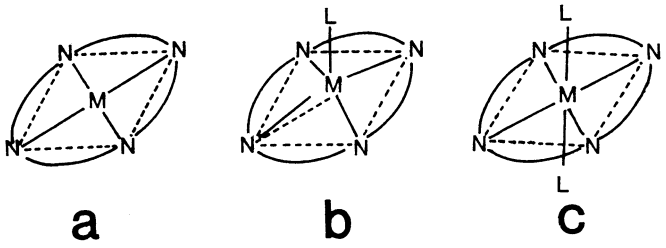

Fig. 10. Schematized representation of the various coordination geometries which are possible for metallophthalocyanines: (a) four-coordinate square planar; (b) five-coordinate square pyramidal; (c) six-coordinate [35].

$$p = F/A = 2nmv_x^2 \tag{2}$$

By considering the rate averages [37]:

$$\langle v_x^2 \rangle = \langle v_y^2 \rangle = \langle v_z^2 \rangle = \tfrac{1}{3}\langle v^2 \rangle \tag{3}$$

$$p = \frac{2}{3} n \left\langle \frac{mv^2}{2} \right\rangle \tag{4}$$

$$\left\langle \frac{mv^2}{2} \right\rangle = \frac{3}{2} kT \tag{5}$$

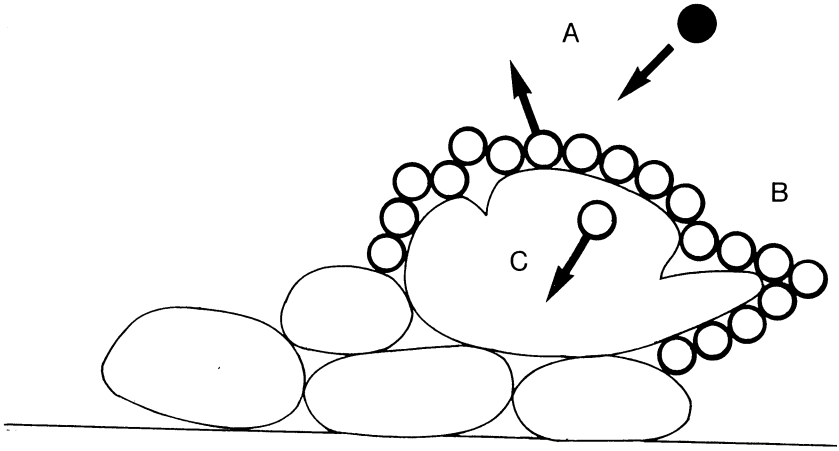

Fig. 11. Schematic representation of some of the physicochemical processes involved in the interaction of gases with a polycrystalline thin film of molecular material. A, displacement; B, defects (structural and chemical); C, intracrystallite diffusion.

$$v_x = \sqrt{\frac{kT}{m}} \tag{6}$$

Therefore, the number of collisions is given by:

$$p/\sqrt{mkT} \tag{7}$$

and the rate of adsorption is:

$$v_{ad}^{+} = \frac{pS}{\sqrt{mkT}} \tag{8}$$

with

$$S = \text{Prob.}\, f(\theta) \exp - \frac{E}{kT} \tag{9}$$

where "Prob." is the probability that a molecule is adsorbed whenever it has both the energy E and a vacant site available, $f(\theta)$ is the probability that the collision arises at a vacant site, and θ is the number of adsorbed molecules divided by the total number of sites.

In the same way, the rate of desorption may be written as:

$$v_{des}^{-} = v_0 f'(\theta) \exp -(E'/kT) \tag{10}$$

where v_0 is a rate constant, and $E' = E + E_{ad}$ (E_{ad} = energy of adsorption).

At equilibrium, for a single species, $v_{ad}^{+} = v_{des}^{-}$, and after some approximations the

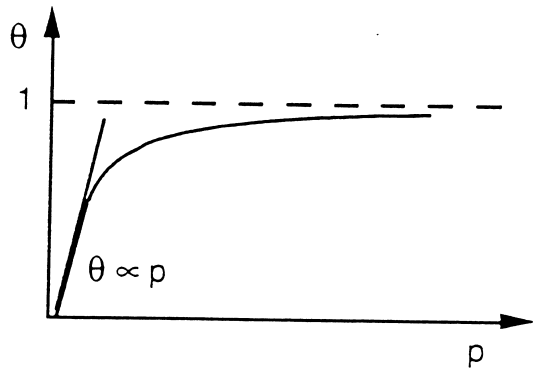

Fig. 12. Percentage of occupied sites as a function of the pressure (reproduced from Ref. [36]).

simple Langmuir isotherm can be obtained:

$$\theta = \frac{ap}{1+ap} \tag{11}$$

with

$$\frac{1}{a} = \frac{v_0}{\text{Prob.}} \sqrt{mkT} \exp - \left(\frac{E_{\text{ad}}}{kT} \right) \tag{12}$$

The term a depends only on the temperature. At low pressures $ap \ll 1$ and Henri's law $\theta = ap$ is obtained (Fig. 12). An increase of temperature will decrease the number of molecules adsorbed at the surface of the molecular material.

A second process, i.e. diffusion within the molecular material must now be considered. The diffusion rate is given by the number of molecules crossing a reference area in a time Δt (it has been shown that it is related to the number of molecules in the volume extending over a distance $v\Delta t$ from the surface). However, backcrossing must also be considered. If n_a is the density of molecules as a function of the position,

$$J_x = -D \frac{\mathrm{d}n_a}{\mathrm{d}x} \tag{13}$$

where D is a diffusion coefficient ($=\mu kT$) and J is the flux of molecules per unit time and surface. An increase in temperature leads to a higher diffusion rate.

The previous equations are not given to establish a quantitative model rationalizing all experimental data. Many approximations have been implicitly taken into account. How can a surface of a polycrystalline material be defined rigorously? Are the sites identical? What are the effects of grain boundaries or structural defects on diffusion processes? Only the qualitative aspects of the processes have in fact been considered.

3.2. Experimental results: monophthalocyanines

The electrical conductivity of molecular materials may be modelled knowing the electrochemical properties of the molecular unit A [38,39]:

$$A \rightleftharpoons A^+ + e^- \quad E^0_{ox}$$

$$A + e^- \rightleftharpoons A^- \quad E^0_{red}$$

The free energy ΔG corresponding to the disproportionation reaction:

$$A,A \rightleftharpoons A^+,A^-$$

is

$$\Delta G = -ne\Delta E$$

where e is the charge on an electron, n is the number of electrons exchanged, $\Delta E = (E^0_{ox} - E^0_{red})$, ΔE in V, ΔG in eV.[2]

From Nernst's law, it can easily be deduced that:

$$[A^-] = [A^+] = [A] \exp - \frac{\Delta G}{2kT} \tag{14}$$

where [A] is the number of molecular units per $cm^3 = (d/M_w)\mathcal{N}$, with d = specific weight ($g\,cm^{-3}$), $\mathcal{N}$ = Avogadro's number, M_w = molar mass of the molecular unit, and k = Boltzmann's constant.

For all molecular materials, with the exceptions of Pc_2Lu and PcLi, ΔG is of the order of 2 eV and, correlatively, the density of intrinsic charge carriers is low and generally negligible at room temperature. By taking $[A] = 10^{21}\,cm^{-3}$, the intrinsically generated concentrations of charge carriers are:

$$[A^+] = [A^-] = 10^4\,cm^{-3}$$

Minute amounts of impurities (I_A) which can act as dopants (electron donors or acceptors) are therefore sufficient to influence the overall conductivity:

$$A,I_A \rightleftharpoons A^+,I_A^-$$

with

$$K = \frac{[A^+,I_A^-]}{[A,I_A]}$$

Even very poor oxidizing and reducing agents can act as dopants. The calculations of the effect of doping agents on the conductivity of molecular materials must, however, take into account the fact that the molecular materials are always polluted

[2] Electron volt (eV) = energy of one electronic charge falling through a potential difference of 1 V (1.602×10^{-19} J).

by dopants fortuitously, or not, present in the thin layers. Dioxygen is one of the most common interfering molecules [40].

Most of the studies concerning PcM-based gas sensors are related to the detection of NO_2, which is a fairly good oxidizing agent, and of interest because of environmental problems.

The importance of the surface on the conductivity of thin films of PcM in the presence of gases has been revealed from the thickness dependence measurements of the conductance [29]. In these types of studies, interdigitated metallic electrodes are used. Gold is thought to yield "ohmic contacts" even though this notion is difficult to define when an interface metal/molecular material is considered [40].

The surface resistance is defined as:

$$R_{\text{surf}} = \frac{V}{I}\frac{1}{L}$$

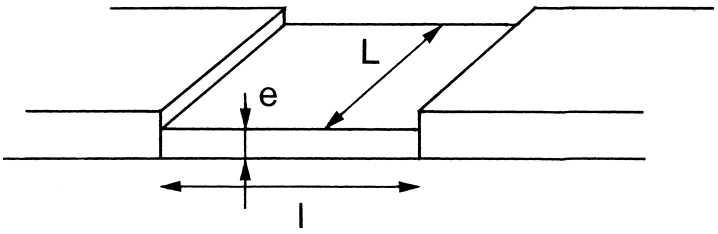

where I is the intensity of the current (in A) corresponding to the voltage (in V), and R_{surf} is in units of V A^{-1}.

Gas sensing properties are highly influenced by various factors, such as [41] film heterogeneities, differences of degree of crystallinity, crystallite size, relative orientation of the crystallites, and grain boundaries. Depending on the adsorption on edges, corners or different sites of structural defects, the gas molecules can be more or less strongly bound.

By comparing the changes of conductivity between PcCu and PcPb induced by an exposure to small amounts of NO_2, it is possible to determine the influence of the morphology of the thin films (Fig. 13).

PcPb and PcCu have very different organizations in thin films. This is clearly reflected in the gas sensing properties: PcPb affords 100-fold faster time responses when the layer is exposed to NO_2 than PcCu (at comparable temperatures but different NO_2 concentrations).

In order to understand the mechanisms which are relevant in NO_2-induced conductivity changes, it is first necessary to determine the effect of O_2 (or air) since this molecule is present in most cases concurrently to NO_2.

Thin films of PcPb ($e < 1000$ nm) have been deposited on SiO_2 or Al_2O_3 in ultra-high vacuum (10^{-8} Torr). The first exposure to O_2 induces orders of magnitude differences in the conductivity of the thin film [43]. Reversible changes upon O_2 exposure in the range 150–200 °C have been found (Fig. 14). O_2 seems to be partly

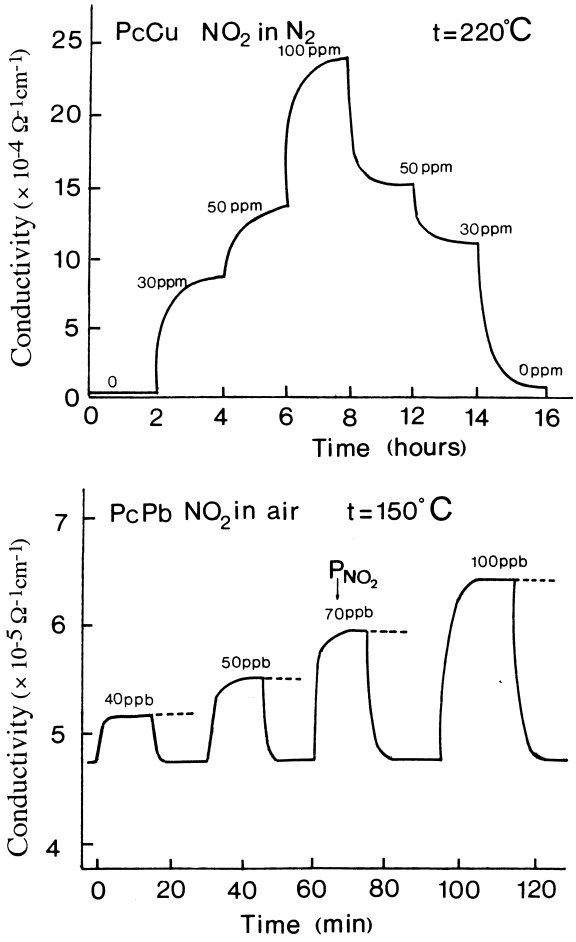

Fig. 13. Conductivity as a function of time of thin films of PcCu and PcPb in the presence of various concentrations of NO_2, after Refs. [42,43]. (It is worth noting that the concentrations of NO_2 differ by a factor of 10^3 between the two experiments: however, for PcCu/NO_2 the kinetics are approximately the same for 2 ppm NO_2.)

incorporated into the bulk of the material, but it also reacts chemically to give surface groups like OH.

The effect of O_2 on PcAlF thin films ($e = 3000$ Å) has been studied by using a quartz microbalance. Within uncertainties, no weight difference of the molecular material layer has been observed in the presence of 100 ppm O_2 in N_2 or in pure O_2 compared with pure N_2. However, at the same time, an important conductivity change is noticed [44]. This probably means that N_2 is displaced by an O_2 molecule which has approximately the same weight but higher electron accepting ability, so a conductivity change is noticed.

The kinetics of O_2 adsorption on PcCo thin films have been studied by Auger

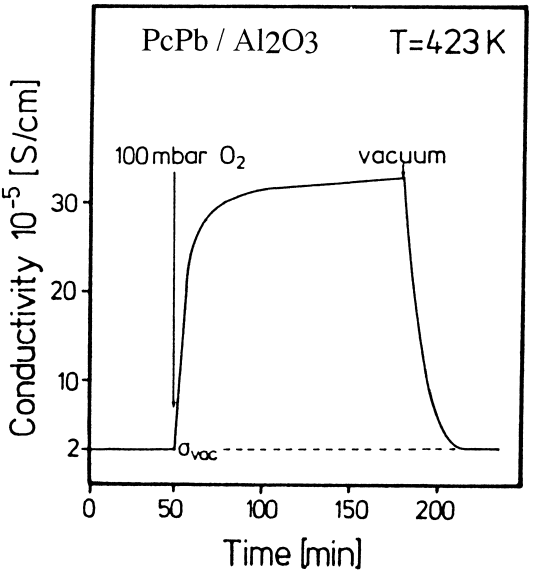

Fig. 14. Effect of O_2 on the conductivity of a PcPb thin film ($e=900$ Å at 150 °C (after Ref. [43]).

spectroscopy (7.4×10^{-8} Torr O_2) [41]. The initial slope corresponds to the adsorption of 5×10^{11} molecules/cm^2 s. After 5 min, corresponding to 35% of the saturation, the slope changes: this is associated with a monolayer coverage of the surface (2×10^{14} molecules/cm^2). Later uptake is related to the rate of transport in the bulk [41].

The fate of the absorbed (and adsorbed) gaseous molecules has been studied via several physicochemical methods: IR, XPS, Auger, etc. [41]. Evidence for the adsorption of H_2O at the four meso-nitrogens of the Pc ring has been found [41]. O_2 on PcPb leads to the appearance of signals corresponding to O_2^- and H_2O [41,45].

The same type of study has been carried out with NO_2 [41,45]. NO_2 exposures show the presence of NO (or bidentate nitrato), NO_3^-, NO_2^- species. In this last case, the metal site seems to be involved in complexation. Thermal desorption studies have been carried out on samples first heated at 150–250 °C under vacuum, then exposed to the gas under consideration at room temperature and then heated up to 300 °C at a constant rate [41]. A single desorption in the range 50–100 °C is noticed for O_2. In the case of NO_2, two peaks are observed around 50–100 °C and 100–250 °C, The desorption is accompanied by the formation of N_2O for $t>150$ °C [41]. Whereas O_2 has a significant but fairly small effect on the conductivity of PcM thin films (×10–100), NO_2 exposures lead to increases of six to eight orders of magnitude [29,47].

The variation of the conductance of PcPb films with time was found to be fairly fast (response time 90%: 90 s) and reversible (recovery time: 140 s) (Fig. 15) [48].

These characteristics are only obtained for temperatures in the range 100–170 °C and for moderate concentrations of NO_2. It has been found that at least two different

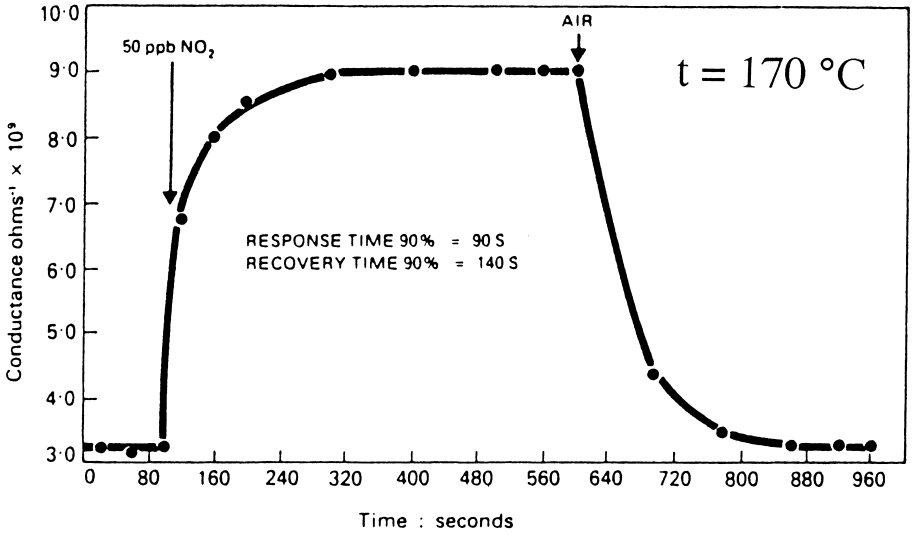

Fig. 15. Variation of the conductance of a PcPb film at 170 °C ($e = 8000$ Å) under 50 ppb of NO_2 and return to air (after Ref. [48]).

types of binding sites can be characterized [49]. At low concentrations of NO_2, adsorption occurs on sites which are weakly bound to the species already present (N_2 or O_2 in most cases). Their replacement, which does not take much time and much energy, can occur at low concentrations of NO_2. This process is satisfactorily reversible (see also Fig. 13).

At high NO_2 contents, NO_2 can displace molecules at sites where they are firmly bound. These sites are responsible for the slow processes which can intervene in the detection. A way to get rid, at least partially, of the second sites is to treat the PcPb layers in air at 360 °C where their destructive oxidation is thought to occur [49,50]. The molecular thin films then lead to a smaller but faster response to NO_2.

The simultaneous measurement of the weight change (quartz microbalance) and of the conductivity has been carried out for thin films of PcAlF ($e = 3000$ Å) submitted to 100 ppm of NO_2 in N_2 at room temperature (Fig. 16).

The mass variations detected by the quartz microbalance strictly follow the conductivity changes since NO_2 replaces a lighter molecule (N_2 or O_2) [44]. The mass of NO_2 adsorbed increases with the concentration of NO_2 and between 0.5 and 5 molecules of NO_2 per molecule of PcAlF seem to be present in the material [44].

Phthalocyanine derivatives substituted with crown ether macrocycles [51] are soluble enough in organic solvents to be deposited from solutions. At room temperature, significant conductivity increases are noticed (with satisfactory reversibility) when the layers are exposed to NO_2 in the range 1–5 ppm. However, after treatment of the molecular thin films with aqueous solutions of KCl, addition of NO_2 leads to a decrease of the conductivity (Fig. 17).

KCl treatment has been shown to yield important changes in the film morphology.

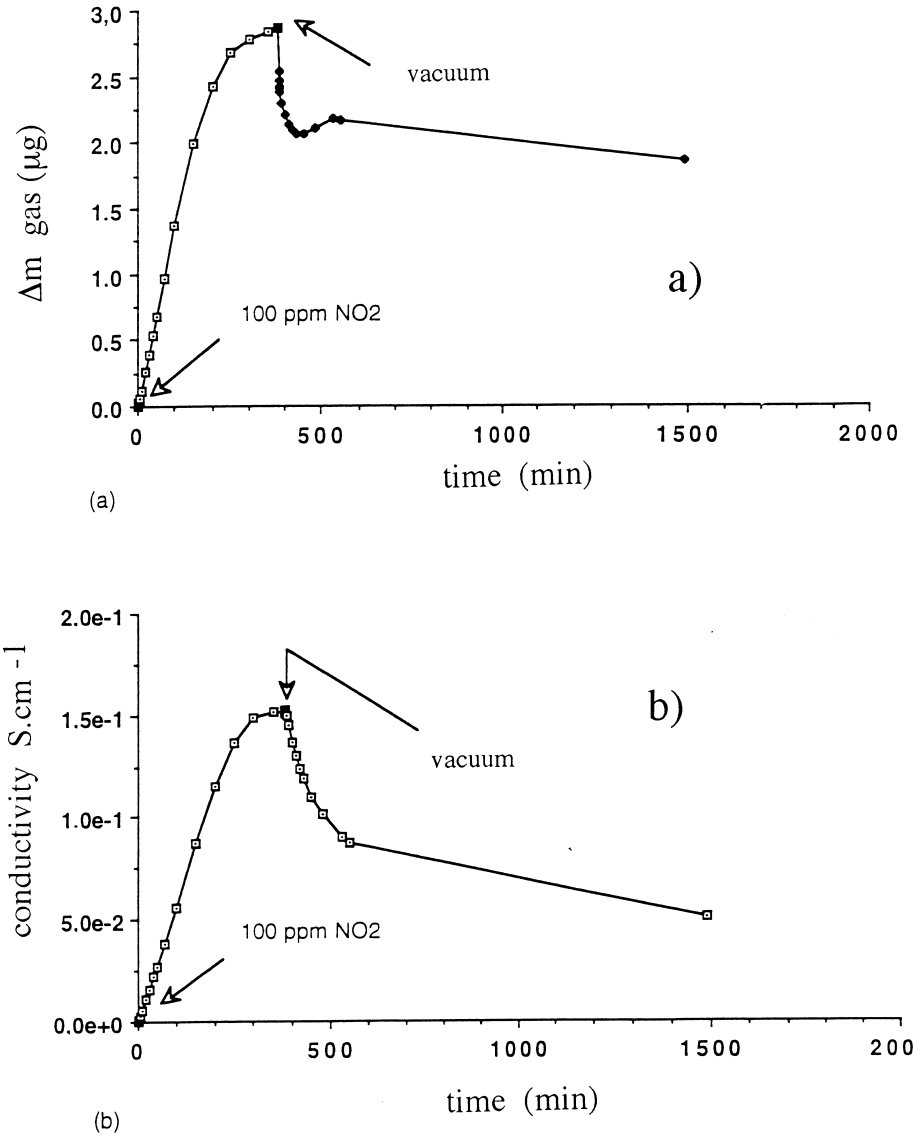

Fig. 16. Thin film of PcAlF ($e = 3000$ Å) submitted to 100 ppm NO_2 in N_2 and then under vacuum: (a) mass variation as a function of time; (b) conductivity change (after Ref. [44]).

No satisfactory model has, however, been given so far to rationalize these results. Other substituted Pc derivatives like tetrachloro [52] or tetrabromo [53] derivatives have been used for NO_2 detection and titration. The addition of NH_3 allows us to reverse the effect of NO_2 or O_2 doping, probably by catalytic chemical removal of the oxidant [54].

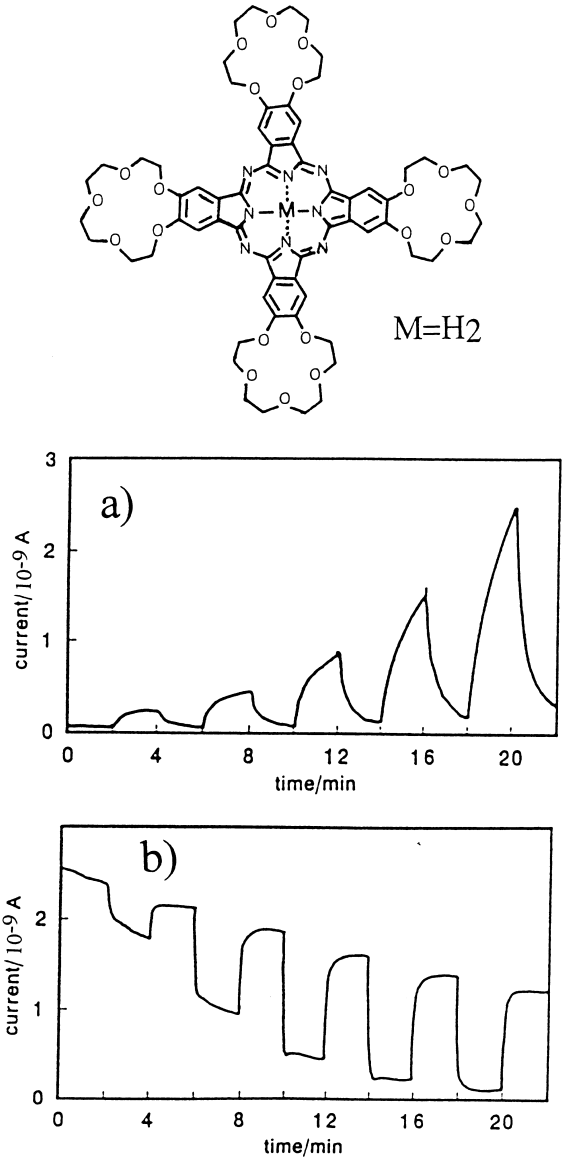

Fig. 17. Chemical formula of the 15-crown-5 derivative of metal-free phthalocyanine and conductivity changes at room temperature upon exposure (a) to clean air for 2 min followed by exposure to 1, 2, 3, 4 and 5 ppm of NO_2 in dry air for 2 min (before KCl treatment), and (b) after KCl treatment (from Ref. [51]).

Ozone (O_3) is an important oxidizing agent which is present in the atmosphere either naturally (photochemical generation) or because of pollution (with synergistic effects with NO_2). Depending on the season, the irradiance or the time of the day,

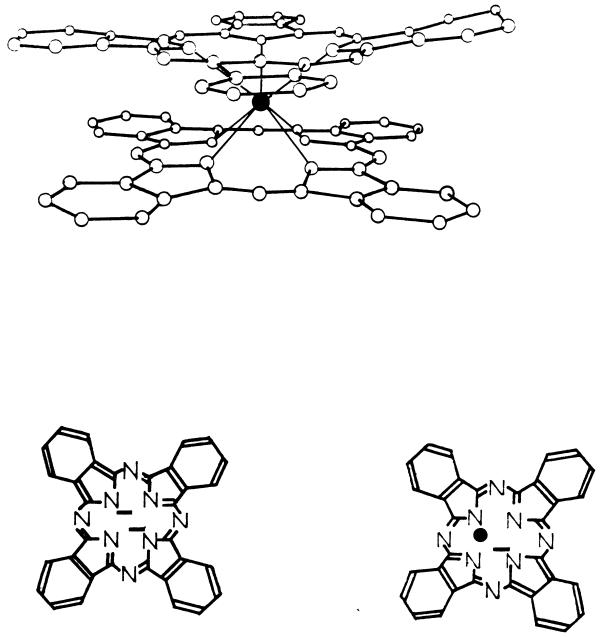

Fig. 18. Molecular structure of rare earth bisphthalocyanine and schematic electronic structure of the two corresponding macrocycles (after Ref. [55]).

Table 2
Difference of redox potentials for mono- and bisphthalocyanines [39,56]

	ΔE_{redox} (V)
PcH_2	1.44
PcCu	1.82
PcNi	1.90
Pc_2Lu	0.48

its concentration can vary in the range 5–50 ppb. The conductivity of thin films of PcCu has been shown to be influenced by the presence of O_3 [134,135]. Satisfactory reproducibility and lifetime were obtained by switching between clean and sample air and by measuring the slope of the resistance during i.e. 1.5 s–1 min, depending on the ozone concentration. Under these conditions, the accuracy was of the order of 5% and the range of concentration of O_3 measurable was 10–5000 ppb [134,135].

3.3. Experimental results: bisphthalocyanines

Rare earth bisphthalocyanines have different molecular and electronic structures compared with those of divalent ion complexes of monophthalocyanines (Fig. 18).

Lutetium bisphthalocyanine, like other rare-earth complexes, is far more easily

oxidized and reduced than the monophthalocyanine derivatives [39,56] (Table 2) because $\Delta E_{redox} = (E^0_{ox} - E^0_{red})$ is smaller than for usual PcMs. As a consequence, the density of intrinsically generated cations and anions (which act as charge carriers) is higher for Pc_2Lu than for PcM and can be detected by conductivity measurements:

$$2Pc_2Lu \rightleftharpoons Pc_2Lu^+ \quad Pc_2Lu^-$$

$$[Pc_2Lu^+] = [Pc_2Lu^-] \approx 9.1 \times 10^{16} \text{ carriers/cm}^3$$

A second difference is due to the morphology of the thin films obtained by vacuum sublimation. In the case of Pc_2Lu [57] the structure of thin films deposited under vacuum (10^{-6} Torr) depends on the thickness of the molecular layer. For films thinner than 600 Å, no electron diffraction is observed and a quasi-amorphous state can be postulated. In the range 600–1000 Å sharp diffraction rings appear. At larger thicknesses, the diffraction rings become discontinuous corresponding to the growth of bigger crystals. The crystals formed are associated with a tetragonal cell ($a = b =$ 19.8 Å, $c = 6.6$ Å). In this structure, the phthalocyanine macrocycles form columns (c-axis). In the crystallites, the columns are mainly parallel to the plane of the substrate. Surprisingly, the conductivity of the quasi-amorphous phase ($10^{-5}\,\Omega^{-1}\,\text{cm}^{-1}$) is not very different to that of the α-form ($9 \times 10^{-5}\,\Omega^{-1}\,\text{cm}^{-1}$, 2000–5000 Å crystallite diameter) [57]. The effect of NO_2 on Pc_2Lu thin films is quite different compared with monophthalocyanine results [58] (Fig. 19).

In a first stage, NO_2 acts as a dopant and Pc_2Lu is partially transformed into Pc_2Lu^+. For the usual metallophthalocyanines, the oxidized amount remains extremely small. In the case of Pc_2Lu, on the contrary, NO_2 can gradually transform a great part of the molecular material into Pc_2Lu^+. The charge transport is given

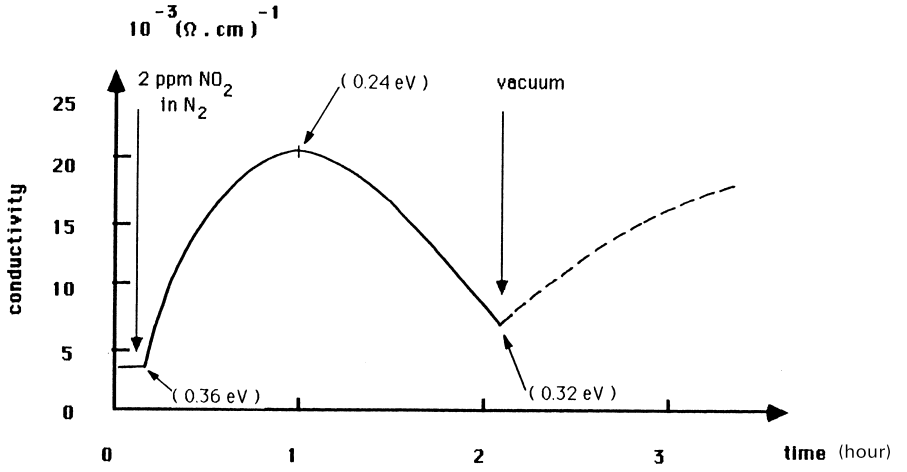

Fig. 19. Conductivity as a function of time for Pc_2Lu thin films in the presence of 2 ppm NO_2 at room temperature (the thermal activation energies of conduction E_{act} in $\sigma = \sigma_0 \exp(-E_{act}/2kT)$ are given in parentheses) [58].

by the following equilibrium when all the material is oxidized:

$$2Pc_2Lu^+ \rightleftharpoons Pc_2Lu, \quad Pc_2Lu^{2+}$$

This reaction requires much more free energy than:

$$2Pc_2Lu \rightleftharpoons Pc_2Lu^+, \quad Pc_2Lu^-$$

Therefore, after the initial increase in conductivity, the conductivity decreases to values lower than the initial one. When the material is not completely oxidized the decrease of σ can also be interpreted as a drop in the mobility of carriers. Evacuation under vacuum at least partly retransforms Pc_2Lu^+ into Pc_2Lu.

The effect of the morphology of the thin film may also be determined by comparing the properties of Pc_2Lu and NPcPcLu. This latter compound is obtained by reacting equimolecular concentrations of phthalonitrile and 2,3-naphthalonitrile with lutetium acetate [136]. This compound affords only quasi-amorphous thin films because it is constituted of several isomers and products. The time response to NO_2 exposure is characterized by t_{max}, the time necessary to obtain the maximum of conductivity σ_{max} (Table 3).

Amorphous Pc_2Lu and NPcPcLu yield approximately the same time responses, whereas crystalline Pc_2Lu leads to 20 times slower kinetic constants. The oxidization of Pc_2Lu may be completed by using a stronger oxidizing agent, like Br_2:

$$Pc_2Lu \xrightarrow{Br_2} Pc_2Lu^+, \quad Br^-$$

The detection of a reducing agent, like ammonia, may be carried out with such oxidized layers (Fig. 20) [59].

In the same way, H_2O vapor may be detected. In molecular materials, the effective dielectric constant is usually fairly low and ion pairs easily form. The incorporation

Table 3
Time necessary to reach the conductivity maximum for thin films of lutetium phthalocyanine and naphthalocyanine upon exposure of 2 ppm NO_2 at room temperature [42]

Product	t_{max}
Pc_2Lu	
300 Å	32 min
(Quasi-amorphous[a])	
3000 Å	24 h 30 min
(Crystalline[b])	
NPcPcLu′	
1000 Å	50 min
(Amorphous)	

[a]No X-ray diffraction.
[b]Deposited under vacuum on a substrate heated at 200 °C. Approximately the same results are obtained for films deposited at 80 °C. However, some amorphous contribution remains.

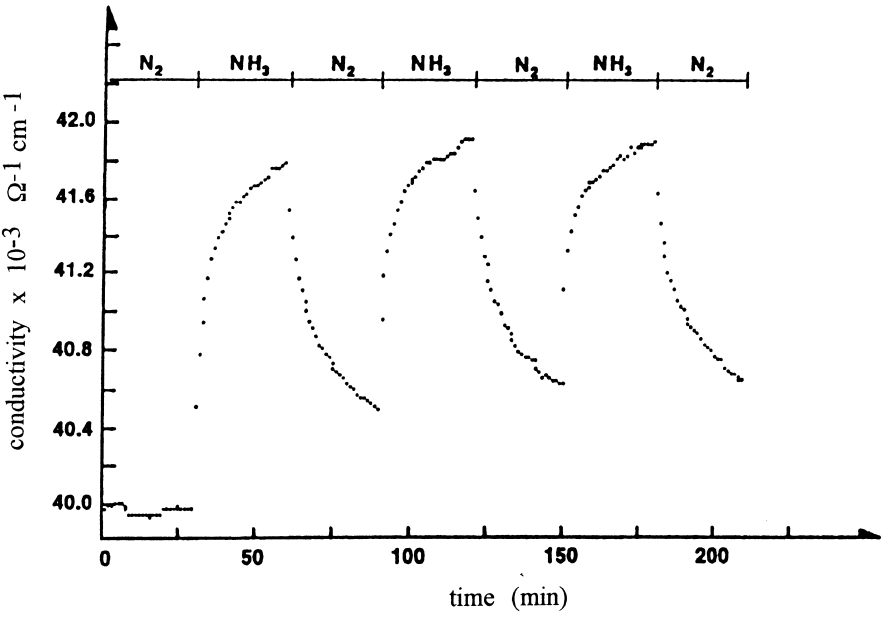

Fig. 20. Conductivity vs. time of a Pc_2Lu film during alternated exposures to 20 ppm NH_3 in N_2 and to N_2 flow at room temperature after oxidation by bromine vapor (after Ref. [59]).

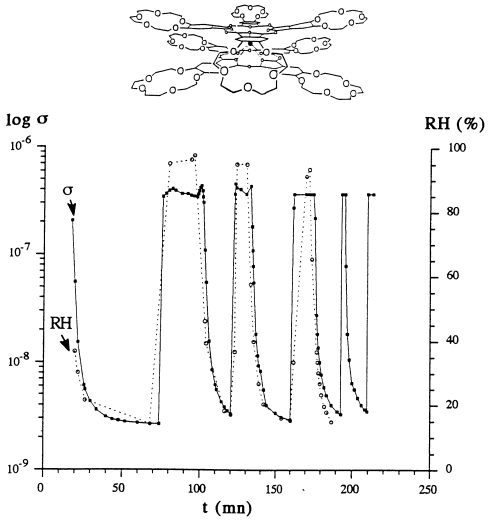

Fig. 21. Conductivity of a $[(15C5)_4Pc]_2Lu$ thin film (thickness 150 Å) successively exposed to a stream of wet and dry nitrogen. The thin film was previously treated with Br_2 (completely oxidized). The relative humidity (RH) was measured with a capacitive humidity sensor [60].

of H_2O molecules within the layer significantly increases the dielectric constant; this in turn facilitates the charge migration (Fig. 21) [60].

3.4. Conclusions and perspectives

Phthalocyanine thin films have been shown to be able to measure low concentrations of gases such as NO_2, O_2, NH_3, H_2O using a conductivity-based device. Both the sensitivity and the reversibility of the detector seem, in some cases, satisfactory. Efforts have to be made to transform the present devices into real sensors.

4. Thin film field effect transistors (FET)

In most previous conductivity measurements, the intensities of current measured are, in most cases, very small. The use of field effect transistors (FET) could permit us to alleviate this difficulty.

4.1. Introduction

In 1947 Bardeen, Brattain and Shockley discovered the first transistor (transresistor) which was 10 times smaller in dimension than the vacuum lamps used at that time. Since then, only mineral derivatives (semiconductors) have been used for making the electronically active layer. In those materials, the electronic levels are collectivized and cannot be associated with single atoms. In molecular materials, the intermolecular interaction energy is fairly small (of the order of kT or less) and electrons and holes are more properly considered as being molecular anions or cations, respectively [38].

Whereas many diode effects (mainly of the Schottky type) have been observed with molecular layers [40], these contacts cannot be compared with those obtained with inorganic materials [61,62]. Efforts to fabricate well-behaved electronic devices

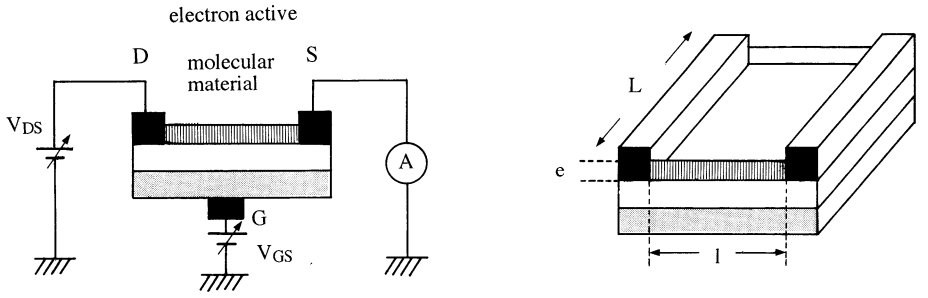

Fig. 22. Schematic representation of a field effect transistor: D, drain; S, source; G, grid (gate); L, width of the metallic electrodes; e, thickness of the molecular material; l, interelectrode spacing (channel length) (modified from Ref. [66]).

seem then to be rather desperate, and one could be tempted to follow W. Pauli's advice [63]:

On semiconductors, one should not do any work …

However, the possibility of making molecular material devices was explored in the authors' laboratories in 1981 [64] and led, following a very sinuous route, five years later to the discovery of molecular FET in 1987 [65].

4.2. Schematic description of field effect transistors

A molecular transcription of the various phenomena involved in FETs can be found. An electron-active molecular material thin film is deposited on a dielectric (SiO_2, Si_3N_4, polymers) of very small thickness (1000–2000 Å) covering a metallic electrode (the grid). Two gold electrodes (source and drain) separated by a distance l are then deposited on the molecular material (Fig. 22).

Let us consider that the molecular material does not possess a significant density of intrinsic charge carriers. When a drain-to-source voltage is applied, no current (or a negligible one) can flow from one electrode to the other. Whenever the energy needed to ensure the disproportionation reaction is too large compared to kT ($kT=$

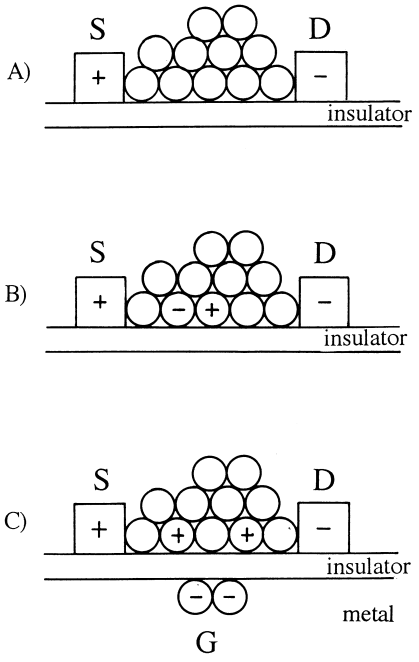

Fig. 23. Three cases which can occur when a potential is applied between two electrodes (source: S; drain: D): (A) the molecular material is a pure insulator; (B) the thermal energy is sufficient to create ion pairs (charge carriers) in the material (intrinsic case); (C) by applying a grid-to-source voltage, charges are generated following $Q=CV$ ($Q_+=Q_-$).

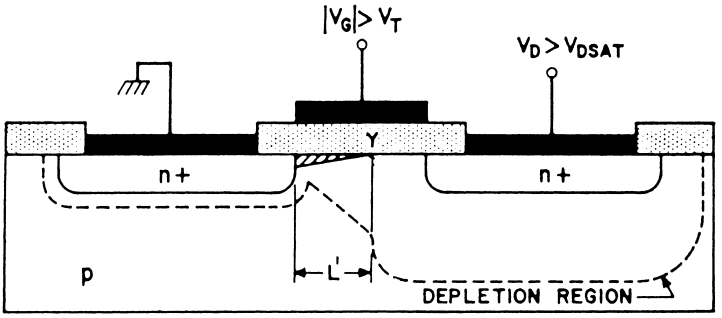

Fig. 24. Schematic representation of a field effect transistor using single crystal silicon-type materials (beyond saturation); V_G and V_D stand for V_{GS} and V_{DS} (after Ref. [67]).

0.0258 eV at RT), the molecular material behaves as an insulator if the quantity of charges injected from the electrodes (injected current) is small [Fig. 23(A) and (B)].

Another mechanism of charge carrier generation may compete or totally replace the previous one if the molecular material is deposited onto a thin dielectric layer covering a conductive electrode (the grid) [Fig. 23(C)]. By applying a potential between the source and the grid, charges are created on the two sides of the insulating layer following the equation $Q=CV$ [where Q is the number of charges (C); C is the capacitance (F); V is the voltage (V)]. The drain-to-source current can therefore be modulated by the grid-to-source voltage.

Conventional field effect transistors based on silicon show very different mechanisms. A simplified scheme is shown in Fig. 24. Above a critical voltage (threshold voltage V_T), the grid can modulate the drain-to-source current. In the absence of grid voltage, no drain-to-source current can flow because two opposite n^+/p diodes are effective at the source and drain electrodes. A depletion region in which the concentration of charge carriers is lower than in the bulk is generated near the source and the drain electrodes. The active layer is a lightly doped mineral semiconductor and, without the rectifying contacts, it should allow charge transport between the source and the drain even without a gate voltage. This type of process does not occur for molecular materials which are insulators (rather than semiconductors) when undoped (with the exceptions of Pc_2Lu and PcLi).

Table 4
Electrical parameters of thin film transistors (TFT) based on amorphous (a-SiH) or polycrystalline (poly-Si) silicon [68] (see also ref. [69])

	a-SiH	poly-Si
μ ($cm^2\ V^{-1}\ s^{-1}$)	0.1–2	10–50
I_{ON} (A)	10^{-5}	5×10^{-6}
I_{OFF} (A)	5×10^{-12}	5×10^{-12}

μ = mobility of charge carriers.
I_{ON}, I_{OFF}, see text.

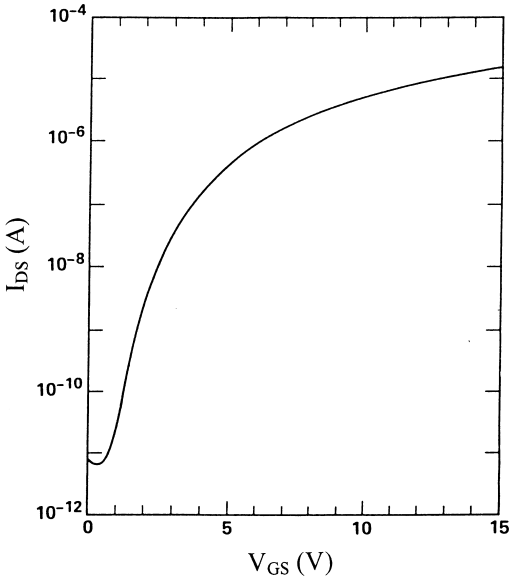

Fig. 25. Drain-to-source current (I_{DS}) as a function of grid-to-source voltage (V_{GS}) for a TFT based on amorphous silicon [68]. Interelectrode spacing 10 μm, width of the electrodes 168 μm, V_{DS} = constant = 15 V.

4.3. Thin film transistors in industry

Silicon is by far the most widely used material for making thin film transistors employed, in particular, in liquid crystal displays. Two important parameters must be taken into consideration: the mobility of charge carriers (which will determine the switching time of the device) and the ratio I_{ON}/I_{OFF}, the drain-to-source intensity of the current in the presence or in the absence of a given grid voltage (Table 4).

The non-linear response of the FET can be more easily visualized by plotting the drain-to-source current I_{DS} as a function of the grid-to-source voltage V_{GS} (Fig. 25). By varying V_{GS} from 1 to 10 V, the corresponding current I_{DS} increases by six orders of magnitude.

It is worth pointing out that the electrical properties of amorphous silicon thin films depend highly on the conditions in which they are fabricated. They are, in most cases, prepared by thermal decomposition of SiH_4. Annealing at 200 °C for 30 min in the absence of light permits us to obtain fairly reproducible electrical conductivities [70]. The undoped thin film conductivity varies from $10^{-11}\ \Omega^{-1}\ cm^{-1}$ to $10^{-5}\ \Omega^{-1}\ cm^{-1}$ depending on the substrate temperature used for the deposition (100 °C and 550 °C, respectively) [70]. Huge efforts have been devoted in the industry to obtaining highly reproducible electrical characteristics for amorphous silicon thin films.

The contacts necessary to have well-behaved transistors have been found to be for instance, a-SiH/n$^+$SiH [71], a-SiH/ITO [72] or a-SiH/metal [73]. However, since a-SiH can be produced with a very low conductivity, a rectifying contact is not always necessary.

The switching time of the FET is given in a first approximation by:

$$T = \frac{l^2}{\mu V_{DS}} \tag{15}$$

where μ is the mobility of charge carriers, l is the interelectrode spacing. It is the time necessary for a charge carrier to go from one electrode to the other. Decent mobilities of charge carriers are therefore necessary to find practical applications. The current–voltage characteristics of the FET may be readily deduced from the basic equations:

$$\sigma = ne\mu \quad \text{and} \quad Q = CV \tag{16}$$

The charge generated in the semiconductor at a distance y from the source is given by:

$$e\Delta n(y) = \frac{C_i}{h}\,[V_{GS} - V(y)] \tag{17}$$

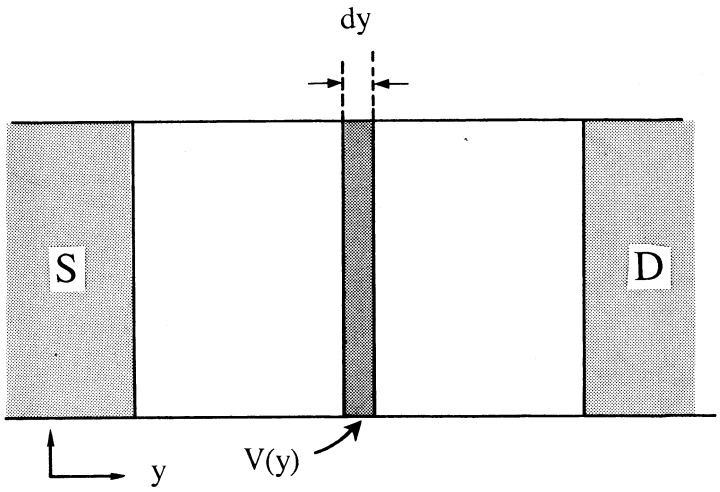

where $\Delta n(y)$ is the excess charge density induced by the grid voltage V_{GS}, C_i is the capacitance of the insulator per unit surface, h is the thickness of the channel (fraction of the thin film thickness e), and $V(y)$ is the potential due to the drain-to-source voltage. $\Delta n(y)$ is the density of charges induced by the field effect in excess

of n_0, the density of charge carriers in the absence of grid voltage. In this last case the corresponding conductivity is σ_0. The drain-to-source current is then given by:

$$I_{DS} = Lh[\sigma_0 + \Delta\sigma(y)]E(y) \tag{18}$$

where L is the width of the electrode, $\Delta\sigma(y) = e\Delta n(y)\mu$, $E(y)$ is the field at abcissa y

$$I_{DS} = Lhe\mu[n_0 + \Delta n(y)]\frac{dV(y)}{dy} \tag{19}$$

In the case where the mobility of charge carriers is the same in the absence or in the presence of field effect and where no injection of charge carriers occurs:

$$I_{DS} = L\mu C_i\left[\frac{ehn_0}{C_i} + V_{GS} - V(y)\right]\frac{dV(y)}{dy} \tag{20}$$

By integrating between $y=0$ and $y=1$, the interelectrode spacing, it becomes:

$$I_{DS} = \frac{L\mu C_i}{l} V_{DS}\left(V_{GS} - V_T - \frac{V_{DS}}{2}\right) \tag{21}$$

with

$$V_T = -\frac{ehn_0}{C_i} \quad \text{(threshold voltage)}$$

When the drain-to-source voltage reaches a certain value, the associated current does not increase any more (saturation current). This corresponds to:

$$\frac{dI_{DS}}{dV_{DS}} = 0$$

The I_{DS}–V_{DS} curve follows a quadratic law until the maximum is reached. At this point, the channel is not continuous any more from the source to the drain. An increase in V_{DS} will decrease the channel length and this effect compensates the expected increase of I_{DS} with voltage (Fig. 26).

At this point the saturation current is obtained, which can be readily calculated from:

$$\frac{dI_{DS}}{dV_{DS}} = \frac{L\mu C_i}{l}(V_{GS} - V_T - V_{DS}) \tag{22}$$

$$\frac{dI_{DS}}{dV_{DS}} = 0 \quad \text{if } V_{DS} = V_{GS} - V_T \tag{23}$$

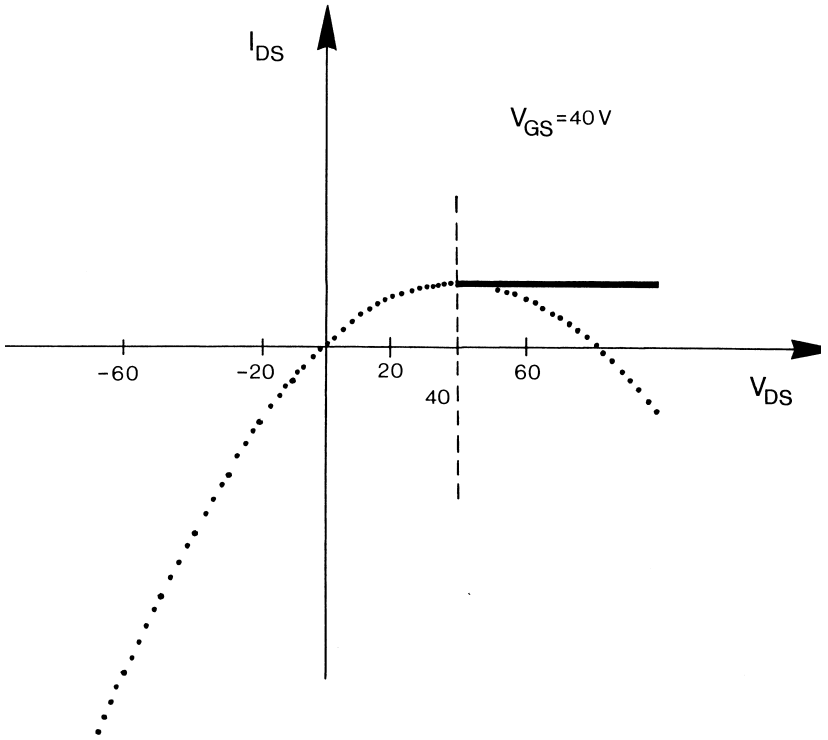

Fig. 26. I_{DS} versus V_{DS}, following Eq. (21), plotted for $V_{GS}=40$ V and $V_T=0$.

Then

$$(I_{DS})_{sat}=\frac{L\mu C_i}{2l}(V_{GS}-V_T)^2 \tag{24}$$

Three other parameters are important to know for characterizing FETs.

(1) The transconductance g_m:

$$g_m=\left(\frac{\partial I_{DS}}{\partial V_{GS}}\right)_{V_{DS}} \tag{25}$$

(2) The drain resistance r_d:

$$r_{\pi d}=\left(\frac{\partial V_{DS}}{\partial I_{DS}}\right)_{V_{GS}} \tag{26}$$

(3) The amplification ratio A:

$$A=g_m r_d \tag{27}$$

The previous equations permit us to interpret the experimental curves, whose typical

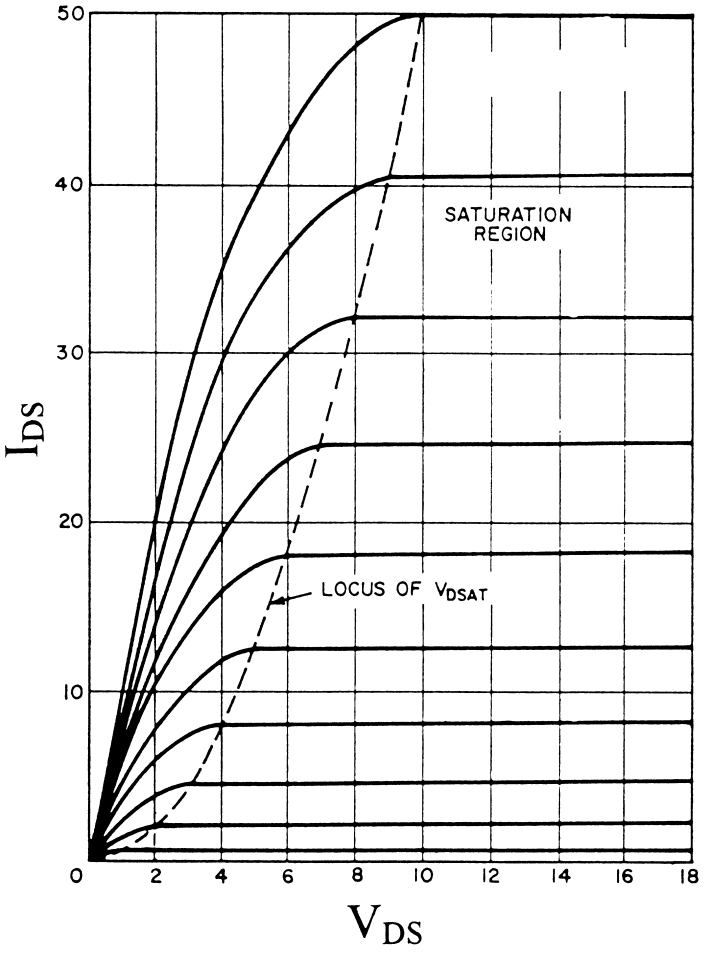

Fig. 27. Drain-to-source current (I_{DS}) as a function of a drain-to-source voltage (V_{DS}) for various grid voltages (V_{GS}) [67].

form is shown in Fig. 27. The charges generated via the grid voltage are not obligatorily all free: some of them can be trapped in structural defects or by impurities:

$$Q = \frac{C_i}{h}[V_{GS} - V(y)] = Q_f + Q_t \tag{28}$$

where Q_f are free charge carriers and Q_t are trapped charge carriers.

$$Q_f = Q - Q_t = \frac{C_i}{h}[V_{GS} - V(y)] - Q_t$$

It can then be demonstrated that Eq. (21) is still valid, but with a different expression of V_T:

$$V_T = -\frac{ehQ_t}{C_i} \tag{29}$$

The threshold voltage can therefore depend on the concentration of trapped charges in the molecular material.

4.4. Molecular field effect transistors: a chronology

The history of molecular field effect transistors is relatively short since the first studies only appeared in the late 1980s. In 1970 [74], it was shown on a single crystal of chloranil that the conductivity of this material can be modulated by a voltage. A few years later [75,76], the same authors described similar studies with tetrathiotetracene. These early publications, however, did not mention the expected saturation effect for a given drain-to-source voltage. In 1983, Ebisawa et al. [77] described the fabrication of an FET based on polyacetylene: the I_{DS} current is indeed modulated by a voltage V_{GS} but no saturation could be observed. In 1987, a group of researchers under the name GRIMM (Groupe de Recherches Interdisciplinaires sur les Matériaux Moléculaires) described the fabrication of a field effect transistor based on lutetium bisphthalocyanines (Pc_2Lu) and zinc monophthalocyanine [65]. Approximately at the same time, field effects on the surface conductivity of metallophthalocyanines were described and the influence of various gases was studied [78] (O_2, I_2, Br_2, etc.). Lead phthalocyanine was also used as the gate of an FET to detect NO_2 [79]. In the same year, a conjugated polymeric material, i.e. polythiophene, was used as the active part of an FET [80]. Very satisfactory characteristics could be obtained already at that time, I_{ON}/I_{OFF} being of the order of 10^2–10^3. Similar studies were then carried out with poly(p-bisphenol) [81]; in this case, the mobility deduced from the FET characteristics was $4 \times 10^{-4}\,cm^2\,V^{-1}\,s^{-1}$ whereas it was around $10^{-3}\,cm^2\,V^{-1}\,s^{-1}$ for polythiophene [82]. Another bisphthalocyanine/monophthalocyanine couple was employed for fabricating FETs [83]. An I_{ON}/I_{OFF} ratio of the order of 10^5 with a mobility of $10^{-4}\,cm^2\,V^{-1}\,s^{-1}$ was described with a polyacetylene-based transistor [84]. More detailed FET characterizations were subsequently reported for the couple Pc_2Lu/PcZn [85–87] or for conjugated polymers [88]. In 1989, the use of an oligomeric form of thiophene (sexithiophene) for making FET was reported [89]. At that time, the I_{ON}/I_{OFF} ratio for the corresponding device was of the order of 2 and the mobilities of charge carriers was low ($3 \times 10^{-4}\,cm^2\,V^{-1}\,s^{-1}$).

In all previous cases, the source and drain electrodes were metallic (in general gold). One publication mentions the use of a conjugated polymer, i.e. polypyrrole, to fabricate the metallic electrodes [90]. However, this did not importantly change the performance of the FET. Around 1990 many papers were published concerning molecular FET [91–127]. It is beyond the scope of this article to detail all of them. In a further section, metallophthalocyanine-based FET will be thoroughly described.

The key points of the published discoveries will be given below for the other compounds.

Langmuir–Blodgett thin films prepared from a mixture of quinquethiophene or poly(3-hexylthiophene) and arachidic acid were used to fabricate a FET [93]. However, very small FET mobilities were obtained ($\mu = 10^{-5}$–7×10^{-7} cm^2 V^{-1} s^{-1}).

Alkyl-substituted polythiophene derivatives soluble in organic solvents were synthesized; they can be deposited by casting, evaporation or spin coating. These materials have been used for fabricating FETs [111–113].

The insulating layer has been replaced by an organic polymeric film [95,96] and all-organic thin film transistors were described [95]. Following this line, printing techniques have been utilized to make FETs [119].

Willander et al. demonstrated in 1993 [97] that the mobility of charge carriers for poly(3-alkylthiophene)-based FETs increases with the gate voltage from 1.2×10^{-5} cm^2 V^{-1} s^{-1} for $V_{GS} = -2$ V to 9.2×10^{-5} cm^2 V^{-1} s^{-1} for -4 V. This has been attributed to the creation of new hopping sites. It could also be due to some field assisted detrapping process of charge carriers at the molecular material/insulating layer interface. A more precise study was carried out with PcNi, indicating the same results [120] (see the following section for more details). An analytical model for organic FETs was proposed in which the threshold voltage V_T corresponds to the filling of traps and is (at ^{2}D) equivalent to the trap filling limit voltage in the space charge limited current model [101].

A Schottky-gated FET in which two gold electrodes are deposited on each side of an aluminum electrode (coplanar geometry) was published; the contact between poly(3-alkylthiophene) and aluminum is rectifying. The drain-to-source current is then modulated by a voltage applied on the aluminum electrode [97,98].

Thin films of diamond obtained by chemical vapor deposition and doped with boron were used as active layers in FET [115]. Molecular ionic derivatives were also used [116,117].

Fullerene compounds C_{60} [126] and C_{70} [121] also lead to good FET characteristics with $\mu = 0.08$ cm^2 V^{-1} s^{-1} and $I_{ON}/I_{OFF} = 10^6$ in the first case.

Electronic circuits, for example a NOR gate, have been fabricated using pentacene or poly(thienylenevinylene) as electrically active layers [128]. The most recent papers on this subject can be found in Refs. [137–141].

4.5. Metallophthalocyanine-based field effect transistors

The first metallophthalocyanine-based FET was composed of two layers, one with a fairly high intrinsic conductivity (Pc_2Lu) and the other insulating when undoped (PcZn) [65,85]. While not expected at the time of the discovery, both layers play an important role in the electrical characteristics of the FET. It is easier, at first, to try to understand the FET behavior for single layers. It is also important to take into account the effect of the ambient on the FET characteristics. This is illustrated in Fig. 28.

The exposure of PcM thin films to ambient air yields a drastic effect on the

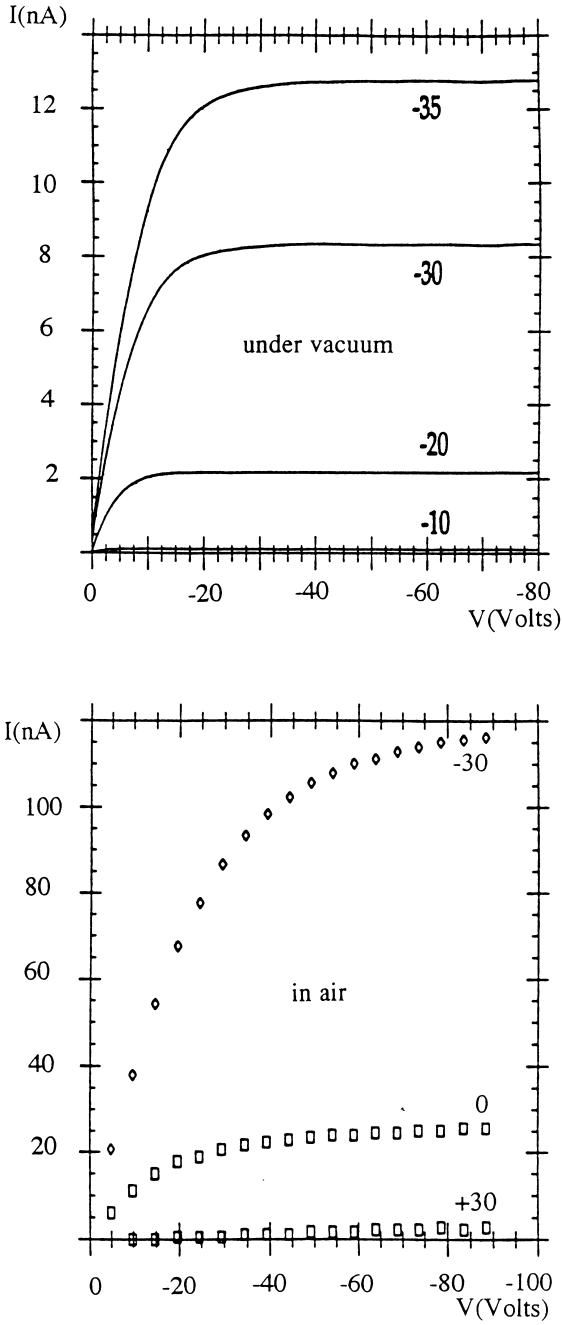

Fig. 28. Curves I_{DS} versus V_{DS} for different grid-to-source voltages (V_{GS}) for a thin film of PcNi ($e = 300$ Å, deposition rate 5 Å s^{-1}). Source-to-drain distance 50 μm, dielectric SiO_2/Si_3N_4 (after Refs. [129,130]) (measurements: ramp voltage 500 ms). (I and V stand for I_{DS} and V_{GS}.)

electrical properties of the FET characteristics as compared to those determined in vacuum. Whereas a negligible current is observed at $V_{GS}=0$ under vacuum, a significant current can be observed in air [129,130].

Several classical mechanisms compete (at $V_{GS}=0$).

– Intrinsic generation of charge carriers: this process is negligible at room temperature for the experiments carried out under vacuum.

– Extrinsic generation of charge carriers. Doping in air (with O_2 or chemically related species) can yield charge carriers following:

$$PcM,O_2 \rightleftharpoons PcM^+, \quad O_2^{-\cdot} \overset{PcM}{\rightleftharpoons} PcM, \quad O_2^{-\cdot} + PcM^+$$

– At sufficiently high V_{DS} voltages, injection of charge carriers from the electrodes is possible. The importance of this contribution has been outlined in the first publications concerning molecular FET [65,85]. The probability of electron transfer from (or to) the electrode to (or from) the molecular material depends on the energy difference between the Fermi level of the metal and the HOMO and LUMO levels of the metallophthalocyanines.

At $V_{GS}<0$, another mechanism of creation of charge carriers is possible in which positive charges are generated (PcM^+) in the molecular material layer.

Modulation of the drain-to-source current in air occurs for both positive and negative grid voltages. Since air increases the density of PcM^+ in the metallophthalocyanine layer, a negative gate voltage will further increase this concentration or neutralize the ionized oxidizing impurities I_A.

$V_{GS}<0$

(a) $PcM//gate \xrightarrow[E]{} PcM^+//gate(-)$

(b) $PcM^+, I_A^-//gate \xrightarrow[E]{} PcM^+, I_A//gate(-)$

At $V_{GS}>0$, the same type of ionic species is formed and the threshold voltage V_T corresponds to the total ionisation of the electron acceptor impurities.

$V_{GS}>O$

(a) $PcM//gate \xrightarrow[E]{} PcM^-//gate(+)$

(b) $PcM,I_A \rightleftharpoons PcM^+,I_A^-$

(c) $PcM,I_A//gate \xrightarrow[E_1]{} PcM,I_A^-//gate(+)$

(d) $PcM,I_A^-//gate(+) \xrightarrow[E_2>E_1]{} PcM^-,I_A^-//gate(++)$

Reaction (d) corresponds to the formation of a channel: the conductivity near the interface is ensured by minority carriers.

A device constituted of n-Si/SiO_2 (3000 Å)/PcNi (1000 Å) (source-to-drain spacing 100 μm) [91] has been studied. The I_{DS} versus V_{DS} curves clearly indicate a doping

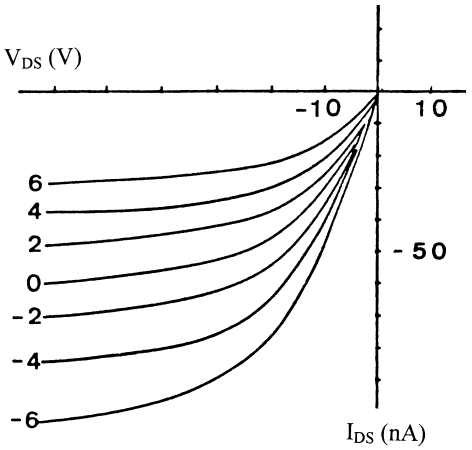

Fig. 29. I_{DS} as a function of V_{DS} for different values of V_{GS} (as indicated). SiO_2: 3000 Å; PcNi: 2000 Å (sublimation rate 60 Å s^{-1}, electrical circuit as in Fig. 22) [91].

by air although the FET characteristics were measured in vacuo [10^{-6} Torr (Fig. 29)]. The PcNi thickness effect on the FET mobilities and on the threshold voltage was studied. Between 100 and 7000 Å, no drastic differences were observed [91].

When the samples are exposed to air, two kinetically different processes take place.

– Quasi-instantaneously, the amplification ratio is lowered, the threshold voltage is increased and the FET mobility decreases.

– After a long time in air (several weeks or months), the value of the threshold voltage decreases to -2 V (instead of -10 V) and the mobility is approximately twice the initial mobility.

A few first conclusions can be drawn.

– There is no diode effect between the source (or drain) electrode and the molecular material.

– The very small intrinsic conductivity of PcNi is the cause of the high resistance at $V_{GS}=0$.

– Charge carriers may be generated by applying a gate-to-source voltage.

– Doping with air (O_2 or related species) increases significantly the conductivity at $V_{GS}=0$.

– PcNi (or PcZn) alone can lead to well-behaved field effect transistors.

It was then necessary to know the FET characteristics of Pc_2Lu thin films. A device constituted of SiO_2 (3000 Å)/Si_3N_4 (2500 Å)/Pc_2Ln (100–400 Å) (Ln = Lu or Tm) was made [92]. The FET characteristics are shown in Fig. 30. The wafers (without Pc_2Lu) were heated in vacuo at 150 °C for 24 h for outgassing. The measurements were made without breaking the vacuum [92].

Pc_2Lu and Pc_2Tm both lead to semiconducting molecular layers with conductivities of $5\times10^{-5}\ \Omega^{-1}\ cm^{-1}$ and $2.5\times10^{-4}\ \Omega^{-1}\ cm^{-1}$, respectively. In this last case, it was suspected that the conduction is not purely intrinsic [92]. It is therefore not

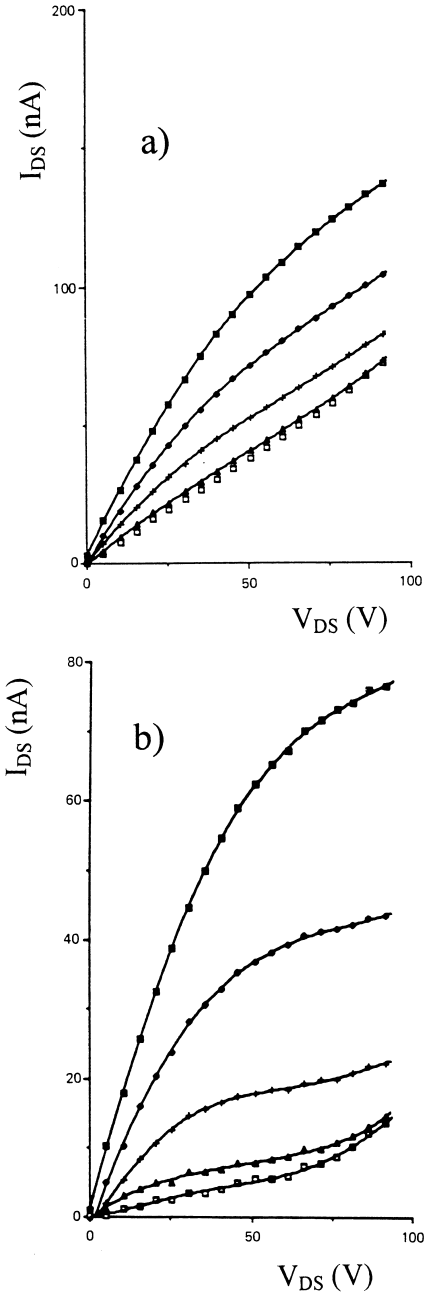

Fig. 30. Intensity of the drain current (I_{DS}) as a function of the drain voltage (V_{DS}) for various grid voltages (V_{GS}) for thin films of Pc_2Lu on Si_3N_4 (measurements under vacuum). □, $V_{GS}=0$ V; ▲, $V_{GS}=10$ V; +, $+V_{GS}=30$ V; ◆, $V_{GS}=50$ V; ■, $V_{GS}=70$ V [92]. (a) Experimental curves, (b) after subtraction of the bulk conductivity.

Table 5
FET characteristics for thin films of Pc_2Lu and Pc_2Tm under various conditions [92]

	Conditions[a]	Carrier	σ_b[b] (Ω^{-1} cm^{-1})	V_T[c] (V)	μ[d] (cm^2 V^{-1} s^{-1})	g_m[e] (nS)	A[f]
Pc_2Lu	1	n	1.5×10^{-5}	8	2×10^{-4}	2.2	50
	2	n, p[g]	4×10^{-4}	1.5	2×10^{-3}	10	100
	3	p	8×10^{-4}	1	3×10^{-3}	14	100
Pc_2Tm	1	n	7×10^{-5}	10	3×10^{-4}	2.8	40
	2	n	1.2×10^{-4}	10	1.4×10^{-3}	16	80
	3	p	3.7×10^{-4}	4	5×10^{-3}	20	40
	4	p	1.2×10^{-3}	4	1.5×10^{-2}	25	20

[a]Conditions: 1, after fabrication in vacuo; 2, after treatment at 150 °C in vacuo; 3, after 2 and exposure to air; 4, after 2 and 3 and annealing in air at 150 °C (2 days).
[b]Bulk conductivity.
[c]Threshold voltage.
[d]Mobility of charge carriers.
[e]Transconductance.
[f]$A = g_m r_d$, with r_d the drain resistance (the bulk conductivity has been subtracted).
[g]The results indicated pertain to the p behavior.

surprising that the drain-to-source current is more than 50 times larger than for PcNi under vacuum and of the same order of magnitude compared to air doped PcNi. The bulk current corresponds for Pc_2Lu to a conductivity of $2.5\times10^{-5}\ \Omega^{-1}\ cm^{-1}$. This calculation is carried out by assuming that the diameter of the channel is negligible compared to the overall thickness of the molecular material. The bulk current flowing relatively far from the interface (more than $\sim$100 Å) is not modulated by the grid voltage.

Modulation is effective with $V_{GS}>0$ and $V_{DS}>0$: this means that a n-type conductivity must be assumed [92]. The stability of the device under vacuum (10^{-6}–10^{-7} Torr) is excellent, with no change in the FET characteristics for several days. However, annealing at 150 °C in vacuo affords both n- and p-type behaviors.

Instead of using Si_3N_4, SiO_2 can be treated with $C_{18}H_{37}SiCl_3$ to remove surface states. Whereas SiO_2 recovered with Pc_2Lu and Pc_2Tm does not show any FET characteristics, surface treated SiO_2 yields n-type FETs under vacuum and p-type in air [92]. The main parameters which can be deduced from the I_{DS}/V_{DS} curves are shown in Table 5. It is worth pointing out that fairly high mobilities ($\mu_{FET}=1.5\times10^{-2}$ cm^2 V^{-1} s^{-1}) have been obtained with a Pc_2Tm thin film annealed at 150 °C in vacuo and at the same temperature in air for two days.

The conclusions of this subsection are therefore as follows.

– Intrinsic molecular semiconductors (Pc_2Lu, PcTm) can be used for fabricating field effect transistors.
– A large bulk current, due to the fairly high intrinsic conductivity of the molecular material, is observed, it cannot be modulated by a grid voltage.
– The drain-to-source current at $V_{GS}=0$ could be reduced if diodes could be

formed at the interfaces between the source and the drain electrodes and the metallophthalocyanine layer.

One can now study the transistor made in 1987 which consisted of two different metallophthalocyanine layers n-Si/SiO_2/PcZn/Pc_2Lu [65,85,86]. In the device most studied [85], the thickness of PcZn and Pc_2Lu was 2000 and 1000 Å, respectively. The metallic electrodes were deposited upon the metallophthalocyanine layers. The FET characteristics obtained are remarkably similar to those expected for a conventional FET [85] (Fig. 31). The molecular FET plots are identical to those obtained with amorphous silicon thin films (Fig. 32) [73].

From Eq. (21), if one transforms $V_{DS} \rightarrow -V_{DS}$ and $V_{GS} \rightarrow V_{GS} - V_{DS}$, one should find $I_{DS} \rightarrow -I_{DS}$. This is indeed the case for the molecular FET as long as $V_{GS} < 0$. However, a non-negligible bulk current (not modulated by the gate voltage) is also observed. The corresponding conductivity σ may be calculated by assuming a spatially homogeneous conduction through the Pc_2Lu layer, the value expected for the bulk is thus found ($10^{-5}\,\Omega^{-1}\,cm^{-1}$). The drain-to-source resistance depends linearly on the thickness of the Pc_2Lu layer and the thermal activation energy of the current is the one expected for pure Pc_2Lu (0.5 eV/$2kT$) [65]. The classical treatments of the data lead to the FET parameters shown in Table 6 together with a comparison with an amorphous silicon based device.

Because of the low mobilities of the charge carriers, the turn-on time of the molecular FET is approximately 10^3 slower than that found for amorphous silicon devices. Taking into account the previous results concerning field effect transistors with single layers of PcNi or Pc_2Lu, the following conclusions can be drawn when both layers are used.

– In the system SiO_2/PcZn/Pc_2Lu, the current which is modulated by the gate voltage arises at the SiO_2/PcZn interface. This SiO_2 layer is at least 10 times more resistive than the PcZn one (under vacuum) .

– Bulk current flowing (relatively) far from the interface goes mainly through the Pc_2Lu layer which has a larger conductivity. This bulk current is not modulated by the gate voltage.

– The electrical properties of the Pc_2Lu layer are close to those previously determined for thin films deposited on glass slides.

Subsequently, very similar studies have been published [83] and patented [131]. The system was SiO_2/PcNi/Pc_2Sc: the results obtained confirmed those previously described. The degree of mixing occuring at the PcNi/Pc_2Sc interface was studied by secondary ion mass spectroscopy (SIMS) as a function of the bisphthalocyanine thickness (300 Å; 1000 Å). It was reported that no clear interface could be seen for the thinner film; the frontier became, however, more pronounced for the thicker layer [83].

It has been recognized, from the very beginning of the studies on FETs, that kinetic effects with long response times occur when the measurements are carried out with d.c. voltages [118].

A drain-to-source voltage varying linearly with time (about 10 V/s) can be used to determine the FET characteristics. In this way perfectly reproducible results are

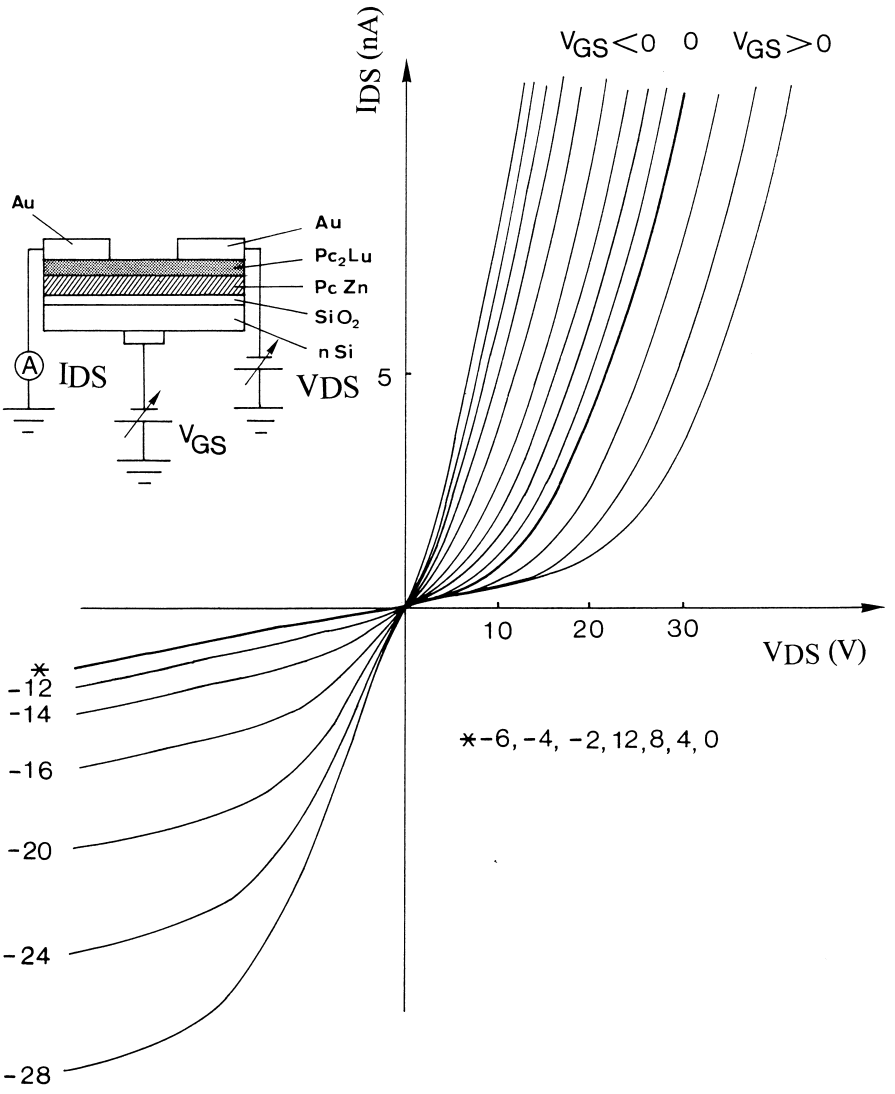

Fig. 31. Intensity–current curves (I_{DS} vs. V_{DS}) as a function of the applied gate voltage (V_{GS}). $V_{GS}>0$: 4, 8, 12 V; $V_{GS}<0$: −2, −4, −6, −12, −14, −16, −20, −24, −28 V for the device shown [85] (ramp = 10 V s^{-1}).

obtained and drift effects are not significant. Measurements have also been carried out with a ramp voltage lasting 500 ms (for approximately 100 V) (Fig. 33).

The measurements shown are made under vacuum and conventional treatment of the data leads to: $\mu = 6.8 \times 10^{-4}$ cm^2 V^{-1} s^{-1}, $V_T = -24.7$ V. The FET mobility is thermally activated and reaches 0.02 cm^2 V^{-1} s^{-1} at 100 °C [118]; this indicates the importance of trapping processes.

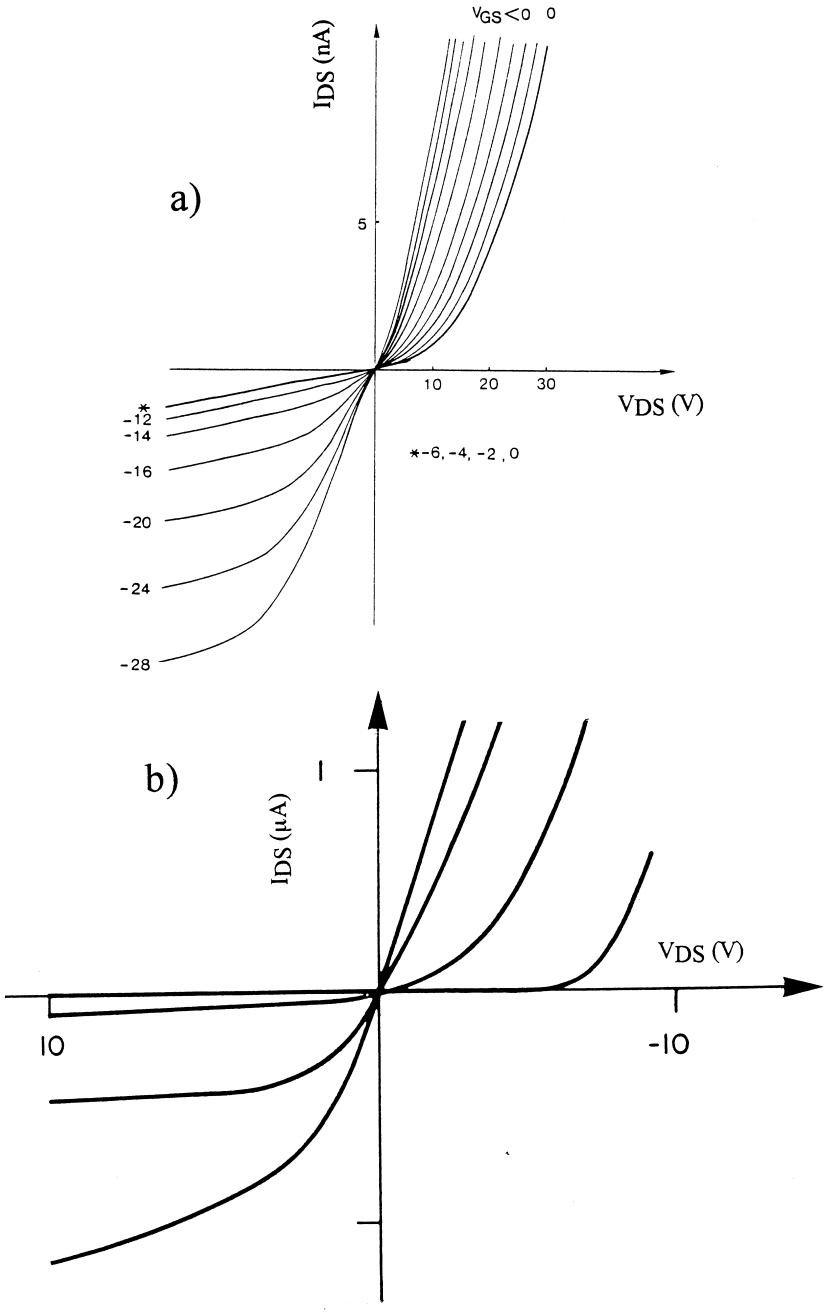

Fig. 32. Drain-to-source current as a function of a drain-to-source voltage for: (a) $SiO_2/PcZn/Pc_2Lu$ device for $V_{GS}<0$ [85]; (b) amorphous SiH FET [73]. $V_T=5$–10 V, $\mu=0.3\ cm^2\ V^{-1}\ s^{-1}$.

Table 6
Comparison of the characteristics of various insulated gate field effect transistors as a function of the semiconductor used (a-SiH: hydrogenated amorphous silicon). μ is the mobility of charge carriers, calculated from the transconductance equation, V_T the threshold voltage, g_m the transconductance, A the amplification factor, and T the turn-on time: $T=l^2/\mu V_{DS}$, calculated with $l=50$ μm (interelectrode spacing), $V_{DS}=10$ V [85]

	Pc_2Lu	a-Si:H
μ ($cm^2\ V^{-1}\ s^{-1}$)	10^{-4}	0.1–2
V_T (V)	−2	−(1–5)
g_m ($A\ V^{-1}$)	0.5×10^{-9}	50×10^{-9}
A	15	65
T	25 ms	1–25 μs

Step voltages have also been applied on the previous molecular FET. To avoid a too important influence of the capacitance term, another electrical circuit has been adopted (Fig. 34).

When the step voltage is applied, at very short times ($t<3$ ms), a current associated with the RC electrical parameters of the circuit is observed. It however takes a longer time (time delay τ) to observe the appearance of a drain-to-source current (Fig. 35).

The time delay τ observed when a step voltage is applied can be interpreted both qualitatively and quantitatively. When a drain-to-source voltage is suddenly applied, the potential within the drain and the gate electrodes is (almost) instantaneously established. In the metallic gate electrode, the charge distribution is such that the potential at any point in the bulk is constant [Fig. 36(a)].

At longer times, the charge migrates in the molecular material driven by the field generated by the source and drain electrodes via a relatively slow hopping process. The countercharge in the gate electrode immediately follows the movement of the charge in the molecular material, or, more properly, the distribution of charges simultaneously rearrange because of the metallic nature of the electrode. Because of those concomitant migrations, no polarization current is observed until the charges reach the counterelectrode. The time needed for the charge to go from one electrode to the other is proportional to the transit time:

$$\frac{l^2}{\mu(V_{GS}-V_T)} \tag{30}$$

where l is the interelectrode spacing, μ is the mobility of charge carriers. A more quantitative treatment was previously proposed in which the device is modelled as shown in Fig. 37.

The time delay τ depends on the drain-to-source voltages, at high values of V_{DS}, it can become of the same order of magnitude as the time constant of the RC electrical circuit (τ_1) (Fig. 38).

The characteristics of the devices are stable for months under vacuum. The time delay is thermally activated and becomes too short to be measured if the temperature

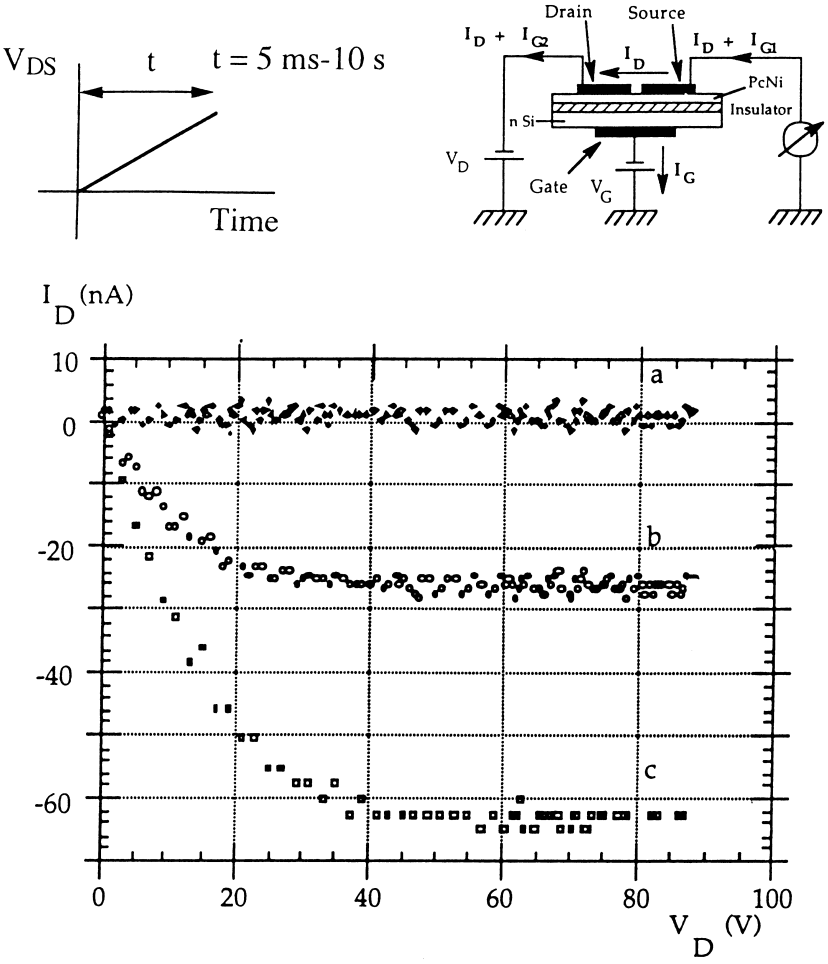

Fig. 33. PcNi drain current as a function of the drain voltage V_{DS} (<0) for various gate voltages V_{GS} (<0). (Scheme a) Drain voltage is a ramp voltage of 500 ms duration. (a) $V_{GS}=0$ V; (b) $V_{GS}=-50$ V; (c) $V_{GS}=-60$ V. The measurements are made without breaking the vacuum at any stage. (In the figure I_D, V_D and V_G stand for I_{DS}, V_{DS} and V_{GS}.)

is higher than 50 °C [118]. The time delay also importantly depends on the time elapsed between two applications of the step voltage (Fig. 39).

This experimental observation clearly indicates that deep traps are present within the material (or, alternatively, polarization of the electrodes could occur). The corresponding thermal detrapping is slow at room temperature but increases with temperature. One of the analytical models describing molecular transistors [101] indicates that "the threshold voltage corresponds to the filling of traps and is a surface equivalent of the trap-filled limit voltage in space-charge limited-current theory".

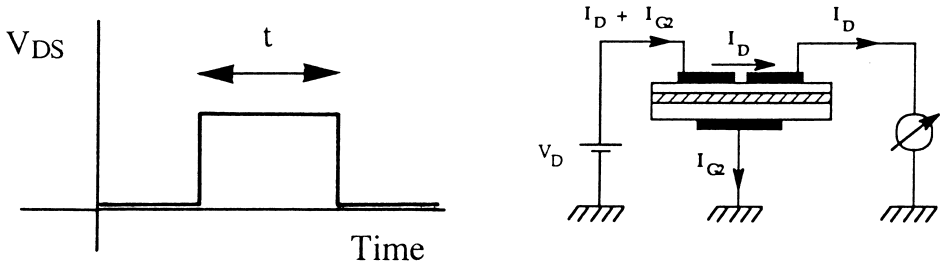

Fig. 34. Electrical circuit used to measure transient currents generated by step voltages (Scheme b) [118]. (V_D, I_D and I_G stand for V_{DS}, I_{DS} and I_{GS}.)

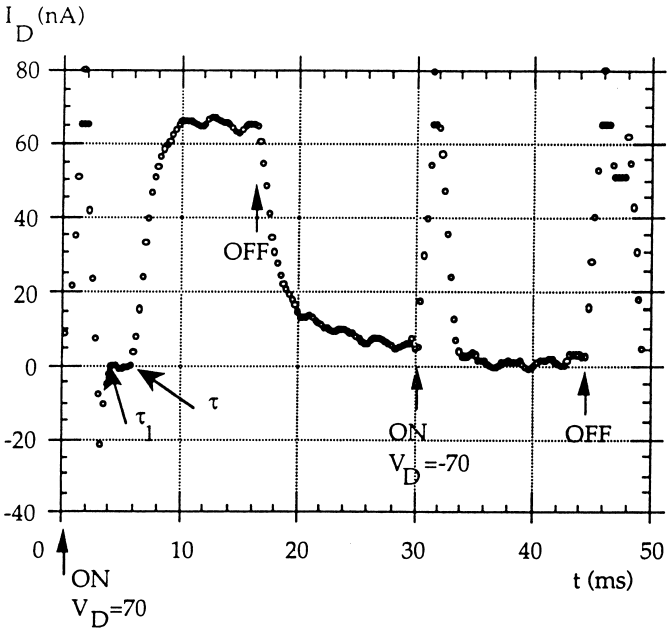

Fig. 35. Drain current as a function of time for different drain voltages (Scheme b). $V_{DS}=70$ V and $V_{DS}=-70$ V. The duration of the pulses is 15 ms. τ_1 = time constant associated with the electrical circuit. τ = delay observed in the appearance of the current [118]. (I_D stands for I_{DS}.)

Further step voltage measurements [120] showed that μ and V_T are not constant as a function of the drain-to-source voltages. It can be demonstrated that the product $T_{DS}\tau$ is given by [132]:

$$0.38C_i(V_{GS}-V_T)1L$$

The curve $I_{DS}\tau$ as a function of V_{DS} is indeed a straight line below 50 V (Fig. 40). By extrapolation of the curve, one obtains $I_{DS}\tau=0$ when $V_{DS}=0$; this indicates that, at least under those conditions, $V_T\approx 0$. This observation differs from the previous

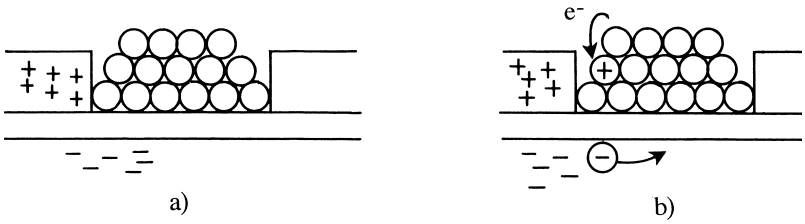

Fig. 36. Schematic representation of the drain-to-source current when a step voltage is applied: (a) step voltage just applied ($t=0$); (b) after a few milliseconds concomitant migration of charges in the molecular material and in the gate metallic electrode occurs.

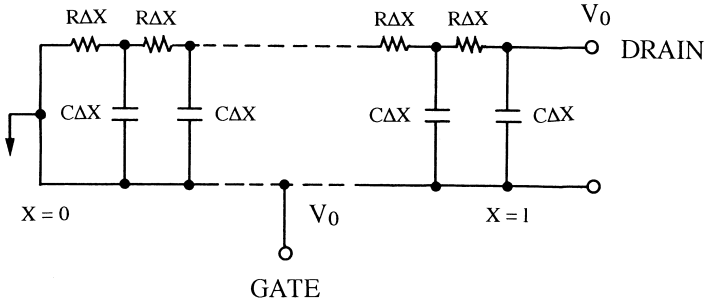

Fig. 37. Electrical circuit used to model field effect transistors. For a thorough development, see Ref. [132].

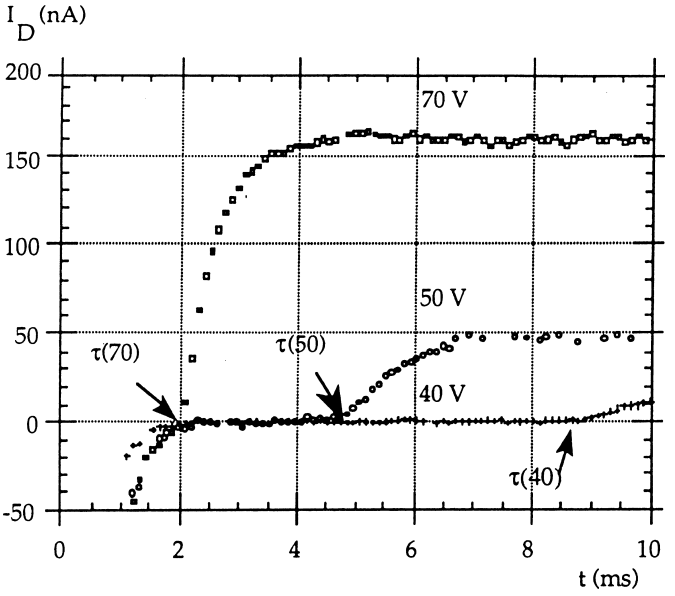

Fig. 38. Drain current as a function of time for different V_{DS}. Pulse duration 15 ms [118]. (I_D stands for I_{DS}.)

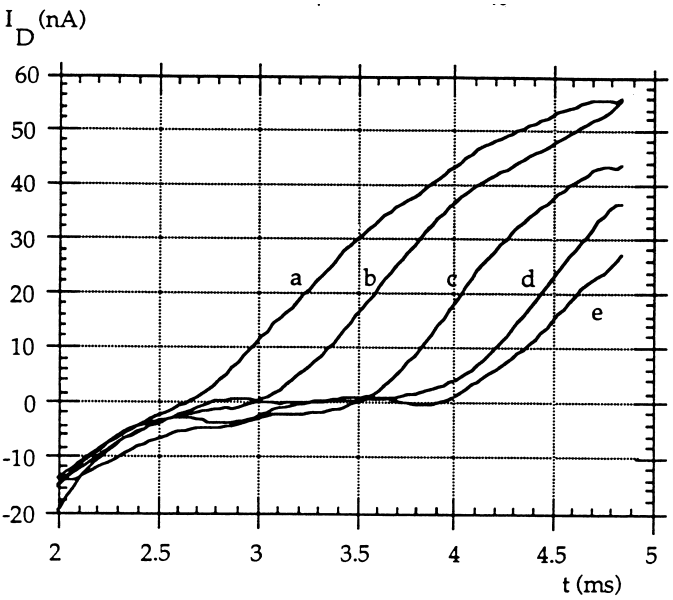

Fig. 39. Drain current as a function of time for $V_{DS}=70$ V. The time elapsed between two pulses has been varied: (a) 15 ms; (b) 30 ms; (c) 100 ms; (d) 500 ms; (e) 1 s. Duration of pulse 15 ms [118]. (I_D stands for I_{DS}.)

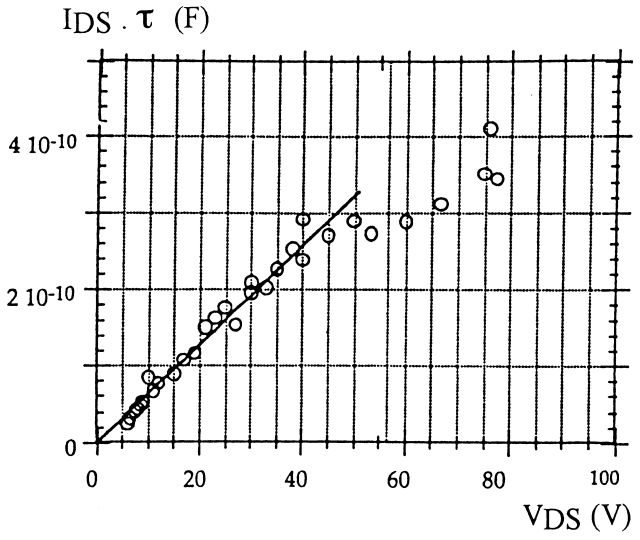

Fig. 40. Dependence of the product $I_{DS}\tau$ on the drain voltage V_{DS} [120].

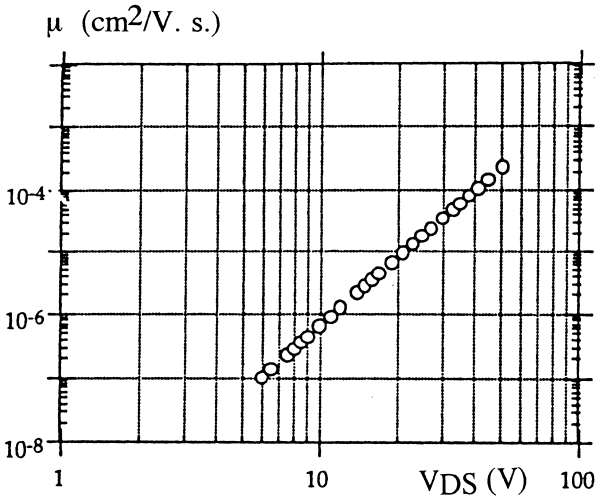

Fig. 41. Dependence of the mobility μ on the drain voltage V_{DS} [120].

determinations using the ramp voltage method. Kinetic effects related to trapping–detrapping processes probably play a role in this apparent discrepancy. The corresponding mobilities can in turn be calculated by assuming $V_T = 0$ (Fig. 41).

Below 50 V, the mobility follows a $V_{DS}^{3.6}$ law, the variation being in the range 10^{-7}–3×10^{-4} cm^2 V/s [120]. In the electrical scheme (b) shown in Fig. 33 and presently used, at any point $V_{DS} = V_{GS}$ the variation of the mobility may therefore be related to a gate-voltage induced filling of traps.

Other experiments have been reported using PcCu [125] or PcM (M = Cu, Zn,

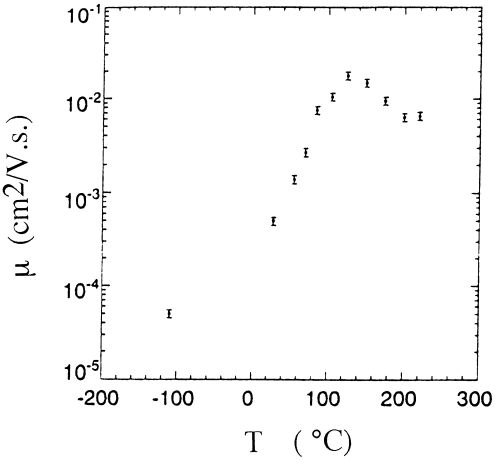

Fig. 42. Field-effect mobility of PcCu at different substrate temperatures. Device n-Si/SiO_2/PcCu (channel lengths 12 and 25 μm) [125]. Rate of deposition = 4–5 Å s^{-1}, pressure = 2.0×10^{-6} Torr.

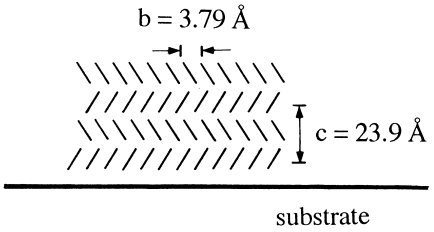

Fig. 43. Schematic representation of the orientation of the molecular units relative to the substrate [125].

Ni, Fe, Sn, Pt, H_2) [127]. The FET characteristics and particularly the mobility of charge carriers (as measured from $\sqrt{I_{DS}}$ vs. $V_{DS}=V_{GS}$ curves) have been shown to be highly dependent upon the temperature of the substrate on which the metallophthalocyanine is deposited. The maximum mobility ($\mu=0.02\ cm^2\ V^{-1}\ s^{-1}$) is found for a substrate temperature around 125 °C (Fig. 42).

In these devices, the I_{ON}/I_{OFF} ratio can reach 4×10^5 [125]. No significant difference in the FET characteristics occurs after long time storage in air, with the exception of a small I_{OFF} increase. X-ray diffraction demonstrated that high temperatures of substrates favor an increase in the sizes of the crystals. The molecular units are probably edge-on relative to the surface (α-form) with the *b*-axis parallel to the substrate (Fig. 43).

By varying the nature of the metal ion, significant differences in the FET mobilities are observed under similar conditions of deposition [127] (Table 7).

The results described so far demonstrate that the molecular material based field effect transistors are original from a fundamental point of view: they differ totally from silicon-based devices for both the charge transport mechanisms (hopping model against band theory) and physicochemical reasons which afford the modulation of the drain-to-source current by a gate voltage. The molecular FET may show fairly good mobilities, high I_{ON}/I_{OFF} ratios and respectable stabilities in air. When rapid switching times are not required, the molecular FET could be used in practical applications. Their cost and ease of fabrication are in their favor compared to amorphous silicon devices. Their use as gas sensors is probably one future application for these molecular FETs. The effect of air on the field induced surface conductivity of PcCu was described already in 1987. Laurs and Heiland also studied gases such as I_2 or Br_2 [78]. A quartz plate (thickness 30 μm) was used as insulating layer. The

Table 7
FET mobilities for a substrate temperature maintained at 125 °C during deposition [127]

PcM	μ ($cm^2\ V^{-1}\ s^{-1}$)
PcCu	2.0×10^{-2}
PcH_2	2.6×10^{-3}
PcZn	2.4×10^{-3}
PcNi	3.0×10^{-5}
PcPt	1.5×10^{-4}

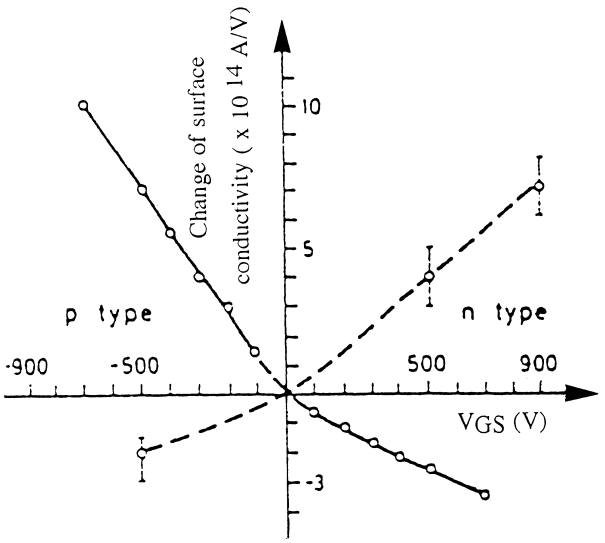

Fig. 44. Change of surface conductivity for PcCu thin films. The coverage is 4.8×10^{16} cm^{-2}; it is considered that the large cross-section of one molecule is 10^{-14} cm^2. n-Type: PcCu doped by deposition of lithium; p-type: O_2- (or another oxidant) doped PcCu (after Ref. [78]).

surface conductivity as a function of the grid voltage was then measured [78] (Fig. 44).

It is reported, with no details, that the "field effect … of p- and n-type films increased by several orders of magnitude with the dark conductivity". Mobilities derived from field effect measurements were in the range 10^{-9}–10^{-5} cm^2 V^{-1} s^{-1} [78].

The metallophthalocyanine may also be used as a gate in FETs. This type of device has been employed to detect NO_2 at concentrations of the order of 1 ppb with a PcPb thin layer [79]. A similar device using Langmuir–Blodgett thin films of porphyrin derivatives has been utilized to detect NO_2, NH_3, CO, H_2S [133].

References

[1] A. Braun, J. Tcherniac, Ber. Deutsch. Chem. Ges. 40 (1907) 2709.
[2] H. De Diesbach, E. Von der Weid, Chim. Helv. 10 (1927) 886.
[3] R.P. Linstead, J. Chem. Soc. (1934) 1016, 1031.
[4] E.A. Lawton, J. Phys. Chem. 62 (1958) 384.
[5] R.P. Linstead, F.T. Weiss, J. Chem. Soc. (1950) 2981.
[6] A.B.P. Lever, Adv. Inorg. Radiochem. 7 (1965) 27.
[7] F.H. Moser, A.L. Thomas, Phthalocyanines, ACS Monograph 157, Reinhold, New York, 1963.
[8] B.D. Berezin, Coordination Compounds of Porphyrins and Phthalocyanines, Wiley, New York, 1981.
[9] K. Kasuga, M. Tsutsui, Coord. Chem. Rev. 32 (1980) 67.
[10] C.C. Leznoff, A.B.P. Lever (Eds.), Phthalocyanines, vols. I–IV, VCH, Weinheim, 1989–1996.

[11] R.P. Linstead, J.M. Robertson, J. Chem. Soc. (1936) 1195, 1636.
[12] J.M. Robertson, R.P. Linstead, C.E. Dent, Nature 135 (1935) 506.
[13] J.M. Robertson, J. Chem. Soc. (1935) 615.
[14] J.M. Robertson, I.J. Woodward, J. Chem. Soc. (1937) 219; (1940) 36.
[15] E. Suito, N. Uyeda, J. Phys. Chem. 84 (1980) 3223.
[16] E. Suito, N. Uyedo, Kolloid Z.Z. Polym. 193 (1963) 7.
[17] J.H. Sharp, M. Lardon, J. Phys. Chem. 72 (1968) 3230.
[18] G. Susich, Anal. Chem. 22 (1950) 425.
[19] F.R. Tarantino, D.H. Stubbs, T.F. Cooke, L.A. Melsheimer, Am. Ink. Maker 29 (1950) 35, 425.
[20] A.A. Ebert Jr.,, H.B. Gottlieb, J. Am. Chem. Soc. 74 (1952) 2806.
[21] F.W. Karasek, J.C. Decius, J. Am. Chem. Soc. 74 (1952) 4716.
[22] M. Shigemitsu, Bull. Chem. Soc. Jpn. 32 (1959) 607.
[23] T. Kobayashi, Y. Fujiyoshi, F. Iwatsu, N. Uyeda, Acta Crystallogr. A37 (1981) 692.
[24] M.S. Mindorff, D.E. Brodie, Can. J. Phys. 59 (1981) 249.
[25] R.D. Gould, J. Phys. D: Appl. Phys. 9 (1986) 1785.
[26] Z. Shi, Q. Yang, L. Chang, Kexue Tongbao 31 (1986) 1108.
[27] K.F. Schoch Jr.,, J. Greggi Jr.,, T.A. Temofonte, J. Vac. Sci. Technol. A6 (1988) 155.
[28] T. Kobayashi, Y. Fujiyashi, N. Uyeda, Acta Crystallogr. A38 (1982) 356.
[29] A.W. Snow, W.R. Barger, in: C.C. Leznoff, A.B.P. Lever (Eds.), Phthalocyanines, vol. I, VCH, Weinheim, 1989.
[30] F. Iwatsu, T. Kobayashi, N. Uyeda, J. Phys. Chem. 84 (1980) 3223.
[31] K. Ukei, Acta Crystallogr. B29 (1973) 2290.
[32] Y. Iyechika, K. Yakushi, I. Ikemoto, H. Kuroda, Acta Crystallogr. B38 (1982) 766.
[33] F. Przyborowski, C. Hamann, M. Müller, C. Reinhardt, M. Starke, W. Vollmann, Wiss. Z. Techn. Hochschule Karl-Marx-Stadt 7 (1980) 709.
[34] F. Przyborowski, C. Hamann, Cryst. Res. Technol. 17 (1982) 1041.
[35] L.J. Boucher, in: G.A. Melson (Ed.), Coordination Chemistry of Macrocyclic Compounds, Plenum Press, New York, 1979.
[36] S. Ross, J.P. Olivier, On Physical Adsorption, Wiley Interscience, New York, 1964; cited in M. Passard, Thèse de doctorat, Université B. Pascal, Clermont Ferrand, 1995.
[37] Feynman/Leighton/Sands, Le Cours de Physique de R.P. Feynman, Mécanique 2, InterEditions, Paris, 1979 (French transl.).
[38] E.A. Silinsh, M. Bouvet, J. Simon, Mol. Mater. 5 (1995) 1, 255.
[39] P. Turek, P. Petit, J.-J. André, J. Simon, R. Even, B. Boudjema, G. Guillaud, M. Maitrot, J. Am. Chem. Soc. 109 (1987) 5119.
[40] J. Simon, J.-J. André, Molecular Semiconductors, Springer, Berlin, 1985.
[41] J.D. Wright, Progr. Surf. Sci. 31 (1981) 1.
[42] M. Passard, Thèse de doctorat, Clermont-Ferrand, 1995.
[43] H. Mockert, D. Schmeisser, W. Göpel, Sensors and Actuators 19 (1989) 159.
[44] C. Maleysson, D. Bouché-Pillon, O. Tomas, J.P. Blanc, S. Dogo, J.P. Germain, M. Passard, A. Pauly, Thin Solid Films 239 (1994) 161.
[45] J.D. Wright, Mater. Sci. 13 (1987) 295.
[46] G. Tollin, D.R. Kearns, M. Calvin, J. Chem. Phys. 32 (1960) 1013.
[47] R.L. van Ewyk, A.V. Chadwick, J.D. Wright, J. Chem. Soc., Faraday Trans. I 76 (1980) 2194.
[48] B. Bott, T.A. Jones, Sensors and Actuators 5 (1984) 43.
[49] A. Wilson, J.D. Wright, Mol. Cryst., Liq. Cryst. 211 (1992) 321.
[50] A. Wilson, G.P. Rigby, J.D. Wright, S.C. Thorpe, T. Terni, Y. Maruyama, J. Mater. Chem. 2 (1992) 303.
[51] P. Roisin, J.D. Wright, R.J.M. Nolte, O.E. Sielcken, S.C. Thorpe, J. Mater. Chem. 2 (1992) 131.
[52] G.L. Pakhomov, V.N. Spector, M.C. Anglada, J.M. Ribo, C. Muller, Mendeleev Commun. (1996) 163.
[53] G.L. Pakhomov, D.E. Pozdnyaev, V.N. Spector, Thin Solid Films 289 (1996) 286.
[54] R.A. Collins, K.A. Mohammed, J. Phys. D: Appl. Phys. 21 (1988) 254.

[55] J. Simon, M. Bouvet, P. Bassoul, in: D. Bloor et al. (Eds.), The Encyclopedia of Advanced Materials, Pergamon, Oxford, 1994, p. 1680.
[56] P. Turek, P. Petit, J.-J. André, J. Simon, R. Even, B. Boudjema, G. Guillaud, M. Maitrot, Mol. Cryst., Liq. Cryst. 161 (1988) 323.
[57] P. Bassoul, M. Bouvet, J. Simon, Synth. Met. 61 (1993) 133.
[58] M. Trometer, R. Even, J. Simon, A. Dubon, J.Y. Laval, J.P. Germain, C. Maleysson, A. Pauly, H. Robert, Sensors and Actuators B8 (1992) 129.
[59] M. Passard, J.P. Blanc, C. Maleysson, Thin Solid Films 271 (1995) 8.
[60] P. Bassoul, T. Toupance, J. Simon, Sensors and Actuators B26-27 (1995) 150.
[61] J. Simon, F. Tournilhac, J.-J. André, J. Appl. Phys. 62 (1987) 3304.
[62] B. Boudjema, G. Guillaud, M. Gamoudi, M. Maitrot, J.-J. André, M. Martin, J. Simon, J. Appl. Phys. 56 (1984) 2323.
[63] Letter from W. Pauli to R. Peierls, 1931.
[64] M. Martin, J.-J. André, J. Simon, Nouv. J. Chim. 5 (1981) 485.
[65] M. Madru, G. Guillaud, M. Al Sadoun, M. Maitrot, C. Clarisse, M. Le Contellec, J.-J. André, J. Simon, Chem. Phys. Lett. 142 (1987) 103.
[66] M. Bouvet, Thèse de doctorat, Paris-ESPCI, 1992.
[67] S.M. Sze, Physics of Semiconductors Devices, Wiley, New York, 1969.
[68] M.J. Thompson, J. Vac. Sci. Technol. B2 (1984) 827.
[69] M. Le Contellec, F. Morin, J. Richard, P. Coissard, M. Morel, M. Bonnel, Report LAB/ROC/TIC.
[70] D.E. Carlson, C.R. Wronski, in: M.H. Brodsky (Ed.), Topics in Applied Physics, vol. 36, Amorphous Semiconductors, Springer, Berlin, 1979.
[71] M. Le Contellec, B. Vinouze, F. Richou, J.L. Favennec, J. Herrou, S. Salaun, Eurodisplay '84.
[72] Y. Ugai, Y. Murakami, J. Tamamura, S. Aoki, SID 84 Digest, p. 308.
[73] F. Morin, M. Le Contellec, Displays Jan. (1983) 3.
[74] M.L. Petrova, L.D. Rozenshtein, Sov. Phys. Solid State 12 (1970) 756.
[75] M.L. Petrova, P.N. Zanadvorov, Sov. Phys. Solid State 14 (1972) 1581.
[76] P.N. Zanadvorov, M.L. Petrova, Sov. Phys. Solid State 21 (1979) 1423.
[77] F. Ebisawa, T. Kurokawa, S. Nara, J. Appl. Phys. 54 (1983) 3255.
[78] H. Laurs, G. Heiland, Thin Solid Films 149 (1987) 129.
[79] P.M. Burr, P.D. Jeffery, J.D. Benjamin, M.J. Uren, Thin Solid Films 151 (1987) L111.
[80] H. Koezuka, A. Tsumura, T. Ando, Synth. Met. 18 (1987) 699.
[81] N. Oyama, F. Yoshimura, T. Ohsaka, H. Koezuka, T. Ando, Jpn. J. Appl. Phys. 27 (1988) 448.
[82] A. Tsumura, H. Koezuka, T. Ando, Synth. Met. 25 (1988) 11.
[83] C. Clarisse, M.-T. Riou, M. Gauneau, M. Le Contellec, Electron. Lett. 24 (1988) 11.
[84] J.H. Burroughes, C.A. Jones, R.H. Friend, Nature 335 (1988) 137.
[85] R. Madru, G. Guillaud, M. Al Sadoun, M. Maitrot, J.-J. André, J. Simon, R. Even, Chem. Phys. Lett. 145 (1988) 343.
[86] R. Madru, G. Guillaud, M. Al Sadoun, M. Maitrot, J.-J. André, J. Simon, R. Even, C.R. Acad. Sci. 306 (1988) 1427.
[87] P. Petit, Ph. Turek, J.-J. André, R. Even, J. Simon, R. Madru, M. Al Sadoun, G. Guillaud, M. Maitrot, Synth. Met. 29 (1989) F59.
[88] H. Koezuka, A. Tsumura, Synth. Met. 28 (1989) F59.
[89] G. Horowitz, D. Fichou, X. Peng, Z. Xu, F. Gamier, Solid State Commun. 72 (1989) 381.
[90] H. Koezuka, A. Tsumura, Synth. Met. 28 (1989) C753.
[91] G. Guillaud, R. Madru, M. Al Sadoun, M. Maitrot, J. Appl. Phys. 66 (1989) 4554.
[92] G. Guillaud, M. Al Sadoun, M. Maitrot, J. Simon, M. Bouvet, Chem. Phys. Lett. 167 (1990) 503.
[93] J. Paloheimo, P. Kuivalainen, H. Stubb, E. Vuorimaa, P. Yli-Lahti, Appl. Phys. Lett. 65 (1990) 1157.
[94] G. Horowitz, X. Peng, D. Fichou, F. Garnier, J. Appl. Phys. 67 (1990) 528.
[95] X. Peng, G. Horowitz, D. Fichou, F. Garnier, Appl. Phys. Lett. 57 (1990) 2013.
[96] F. Gamier, G. Horowitz, X. Peng, D. Fichou, Adv. Mater. 2 (1990) 592.
[97] M. Willander, A. Assadi, C. Svensson, Synth. Met. 55 (1993) 4099.
[98] A. Assadi, M. Willander, C. Svensson, J. Hellberg, Synth. Met. 58 (1993) 187.
[99] F. Garnier, X. Peng, G. Horowitz, D. Fichou, Mol. Eng. 1 (1991) 131.

[100] F. Garnier, G. Horowitz, X. Peng, D. Fichou, Synth. Met. 45 (1991) 163.
[101] G. Horowitz, P. Delannoy, J. Appl. Phys. 70 (1991) 469.
[102] G. Horowitz, X. Peng, D. Fichou, F. Gamier, J. Mol. Electron. 7 (1991) 85.
[103] G. Horowitz, D. Fichou, X. Peng, F. Garnier, Synth. Met. 41 (1991) 1127.
[104] G. Horowitz, T. Delannoy, J. Chim., Phys. Phys.-Chim. Biol. 89 (1992) 1037.
[105] G. Horowitz, X. Peng, D. Fichou, F. Gamier, Synth. Met. 51 (1992) 419.
[106] X. Peng, G. Horowitz, F. Garnier, J. Chim. Phys. Phys.-Chim. Biol. 89 (1992) 1085.
[107] F. Garnier, A. Yassar, G. Horowitz, F. Deloffre, Mol. Cryst., Liq. Cryst. 230 (1993) 81.
[108] F. Gamier, A. Yassar, R. Hajlaoui, G. Horowitz, F. Deloffre, B. Servet, S. Ries, P. Alnot, J. Am. Chem. Soc. 115 (1993) 8716.
[109] G. Horowitz, F. Deloffre, F. Gamier, R. Hajlaoui, M. Hmyene, A. Yassar, Synth. Met. 54 (1993) 435.
[110] B. Servet, S. Ries, M. Trotel, P. Alnot, G. Horowitz, F. Garnier, Adv. Mater. 5 (1993) 461.
[111] A. Assadi, C. Svensson, M. Willander, O. Inganas, Appl. Phys. Lett. 53 (1988) 195.
[112] J. Paloheimo, E. Punkka, H. Stubb, P. Kuibalainen, Proc. NATO Adv. Study Inst. Spetses, Greece, 1989.
[113] H. Akimichi, K. Wargai, S. Hotta, H. Kano, H. Sasaki, Appl. Phys. Lett. 58 (1991) 1500.
[114] Y. Ohmori, K. Muro, M. Onoda, K. Yoshino, Jpn. J. Appl. Phys. 31 (1992) L646.
[115] K. Nishimura, K. Kumagai, R. Nakamura, K. Kobashi, J. Appl. Phys. 76 (1994) 8142.
[116] C. Pearson, A.J. Moore, J.E. Gibson, M.R. Bryce, M.C. Petty, Thin Solid Films 244 (1994) 932.
[117] P. Hesto, L. Aguilhon, G. Tremblay, J.P. Bourgoin, M. Vandevyver, A. Barraud, Thin Solid Films 242 (1994) 7.
[118] G. Guillaud, J. Simon, Chem. Phys. Lett. 219 (1994) 123.
[119] F. Garnier, R. Hajlaoui, A. Yassar, P. Srivastava, Science 265 (1994) 1684.
[120] G. Guillaud, R. Ben Chaabane, C. Jouve, M. Gamoudi, Thin Solid Films 258 (1995) 279.
[121] R.C. Haddon, J. Am. Chem. Soc. 118 (1996) 3041.
[122] G. Horowitz, F. Garnier, A. Yassar, R. Hajlaoui, F. Kouki, Adv. Mater. 8 (1996) 52.
[123] A. Dodabalapur, L. Torsi, H.E. Katz, Science 268 (1995) 270.
[124] G. Horowitz, Adv. Mater. 8 (1996) 177.
[125] Z. Bao, A.J. Lovinger, A. Dodabalapur, Appl. Phys. Lett. 69 (1996) 3066.
[126] R.C. Haddon, A.S. Perel, R.C. Morris, T.T.M. Palstra, A.F. Hebard, R.M. Fleming, Appl. Phys. Lett. 67 (1995) 121.
[127] Z. Bao, A.J. Lovinger, A. Dodabalapur, Adv. Mater. 9 (1997) 42.
[128] A.R. Brown, A. Pomp, C.M. Hart, D.M. de Leeuw, Science 270 (1995) 972.
[129] G. Guillaud, R. Ben Chaabane, M. Gamoudi, L'Onde électrique 74 (1994) 14.
[130] G. Guillaud, in preparation.
[131] C. Clarisse, M. Le Contellec, M.-T. Riou, French Patent 87 (1987) 15490.
[132] J.R. Burns, R.C.A. Rev. 68 (1969) 15.
[133] L. Sun, C. Gu, K. Wen, X. Chao, T. Li, G. Hu, J. Sun, Thin Solid Films 120–122 (1992) 486.
[134] A. Schütze, U. Weber, J. Zacheja, D. Kohl, W. Mokwa, M. Rospert, J. Werno, Sensors and Actuators A37A38 (1993) 751.
[135] A. Schütze, N. Pieper, J. Zacheja, Sensors and Actuators B23 (1995) 215.
[136] M. Bouvet, J. Simon, Chem. Phys. Lett. 172 (1990) 299.
[137] A.R. Brown, C.P. Jarrett, D.M. de Leeuw, M. Matters, Synth. Met. 88 (1997) 37.
[138] H.E. Katz, J. Mater. Chem. 7 (1997) 369.
[139] A.J. Lovinger, L.J. Rothberg, J. Mater. Res. 11 (1996) 1581.
[140] A. Dodabalapur, H.E. Katz, L. Torsi, Adv. Mater. 8 (1996) 853.
[141] C.-T. Kuo, W.-H. Chiou, Synth. Met. 88 (1997) 23.